Preparation and photocatalytic activity of TiO$_2$/PPy/GO for the degradation of Rose Bengal and Victoria Blue dye in visible light in aqueous solution

Azad Kumar*, Gajanan Pandey

*Department of Applied Chemistry, School for Physical sciences, Babasaheb Bhimrao Ambedkar University, Lucknow, India,
email: kumarazad20@gmail.com*

ABSTRACT

This research work describes a proficient method for synthesis of TiO$_2$/PPy and TiO$_2$/PPy/GO nanocomposites. These nanocomposites were prepared by one-step in-situ deposition oxidative polymerization of pyrrole hydrochloride using ammonium persulphate as an oxidant in the presence of TiO$_2$ nanoparticles (NPs) cooled in an ice bath. The obtained nanocomposites were characterized by X-ray diffraction, transmission electron microscope, scanning electron microscope, UV-Visible, Brunauer–Emmett–Teller, and photoluminescence spectra techniques. The obtained results showed that TiO$_2$ NPs have been encapsulated by PPy with a strong effect on the morphology of TiO$_2$/PPy and TiO$_2$/PPy/GO nanocomposites. The photocatalytic degradation of Rose Bengal and Victoria Blue dyes were done at different condition viz. concentration of dye, time of illumination, pH, and dose of photocatalyst. The maximum photodegradation of dyes was found at 7 pH, 20 ppm concentration of Victoria Blue and 25 ppm of Rose Bengal dye solution, 800 mg/L for Victoria Blue dye (VB) and 1,600 mg/L for Rose Bengal dye (RB) amount of photocatalyst, and 120 min irradiation of visible light. Kinetics of photodegradation was investigated for VB and RB dye and found first-order kinetics.

Keyword: Photodegradation; Polymerization; Nanocomposites; Rose Bengal; Victoria Blue; Photocatalyst

1. Introduction

The wastewater released from textile and other colouring industries, containing the various dyes, has been badly affecting aquatic life and living organism due to their carcinogenic behaviour. Lots of investigations reported that 10%–12% of dyes, such as Rose Bengal, Victoria decreasing the percentage of degradation blue, Thymol Blue, Caramine, Indigo Red, Red 120, Rhodamine B, Methylene Blue, Eriochrome Black-T, and so on, have been used every year in textile industries [1–4]. The major portion (~20%) of these dyes is lost during synthesis and processing operations, which enter into water bodies through effluents, causing water pollution. Rose Bengal (Fig. 1(a)) is a significant xanthene dye used in textile and photochemical industries. It has severe toxic effects on the human health [5–7] and becomes dangerous in contact with skin, causing itching, irritation, reddening, and blistering. It also affects eyes causing inflammation, eye redness, itching, and so on [8]. Victoria Blue (Fig. 1(b)) is another triphenylmethane-derivatized dye. It has been extensively used as textile dyes for silk, wool, and cotton; in the preparation of inks; in the surface coating and dyeing of paper [9–11]; as colorants in foods, drugs, and cosmetics [12]; as biological stains; and as anti-infective, antimicrobial, and antihelmintic agents [13]. The photocytotoxicity of triphenylmethane dyes is based on the production of the reactive oxygen species and tested extensively with the regard to its photodynamic treatment [14]. The physical properties of dyes are shown in Table 1.

In the past, several techniques, such as coagulation, flocculation, reverse osmosis, adsorption, ion-exchange method, ultra-filtration, and photosensitized oxidation, have been used to reduce the toxic dye effluents from wastewater [15–18]. Though methods are fairly effective in removing pollutants; however, the main drawback of these techniques is the formation of the secondary waste product that cannot be
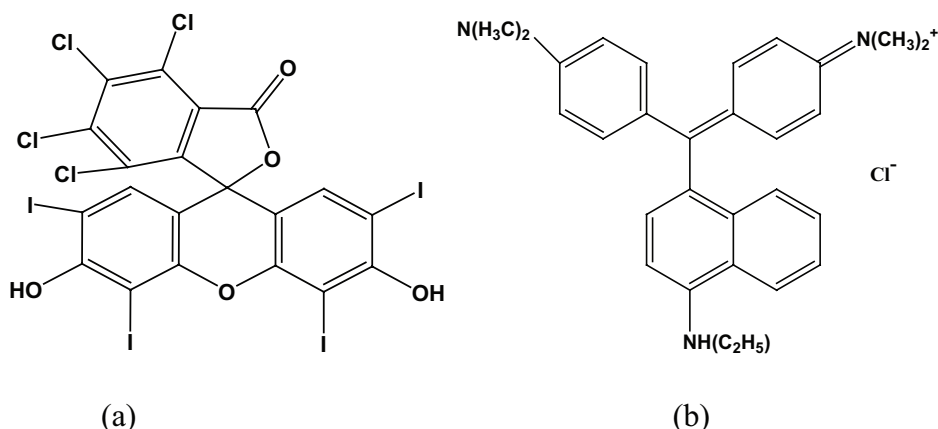
* Corresponding author.

Fig. 1. Molecular structure of dyes: (a) Rose Bengal (b) Victoria Blue.

treated again and dumped as such [19]. In the recent years, photocatalytic degradation has emerged as an effective technique for complete mineralization of wastewater. Titanium dioxide (TiO_2) nanoparticles (NPs) are an excellent photocatalyst because of its low cost, simple preparation, good stability, non-toxicity, and better photodegradation ability [20]. It has successfully been used in solar cells [21], photocatalysis [14], and photocatalytic hydrogen production [22]. The bare TiO_2 NPs have the wide band gap; thus, have low sunlight energy conversion efficiency and high rate of ($e^-–h^+$) electron-hole recombination capability. Therefore, improvement of the photocatalytic properties of TiO_2 is essential. In order to enhance the photocatalytic properties of TiO_2, number of manipulations, such as metal or non-metal doping [23]; compositing with other semiconductors [24]; compositing with conductive materials such as graphene [25] or carbon nanotubes [26]; and sensitization with organic dyes and conductive polymers such as polyaniline [27], polythiophene [28], and polypyrrole (PPy), have been tested in the past [29]. Among these routes, the coating of conductive polymers is one of the most effective methods for the generation of good photocatalytic activity [30]. The coating of conductive polymers can reduce the recombination rate of electron-hole ($e^-–h^+$) simultaneously act as sensitizer making effective large band gap semiconductor like TiO_2 [31,32].

Among the various conductive polymers, PPy is one of the most promising coating agents, owing to its good conductivity, high absorption coefficient in the visible part of sunlight, high charge carrier mobility, and good environmental stability [33]. Therefore, PPy is suitable conducting polymer and stable photosensitizer to improve the photocatalytic activity of TiO_2 in solar light. In the past, TiO_2/PPy nanocomposite has been successively used in solar cells and for the photocatalytic degradation of organic species; however, its use in photocatalytic degradation of organic dyes is rarely reported.

There are many methods of preparing TiO_2/PPy nanocomposite, for example, anodic co-deposition [34], self-assembly techniques [35], photoelectrochemical polymerization [36], and hydrothermal methods [37]. However, in-situ chemical polymerization is a promising method for preparation of TiO_2/PPy owing to its simplicity, good reproducibility, and easy scale-up.

In the present study, TiO_2, TiO_2/PPy, and TiO_2/PPy/ graphene oxide (GO) nanocomposites have been prepared by one-step in-situ polymerization of pyrrole in the reaction medium. The photocatalytic degradation of Victoria Blue and Rose Bengal have been studied in the presence of TiO_2, TiO_2/PPy, and TiO_2/PPy/GO nanocomposites at the different parameters, that is, concentration of dye, the dose of the photocatalyst, pH of the reaction mixture, and irradiation time. The kinetics for the photodegradation process has also been investigated in this work.

2. Experimental methods

2.1. Materials

Pyrrole monomer, having molar mass of 67 g/mol and density of 0.97 g/cm³ (Merck, India), was triple distilled until a colourless liquid was obtained. The distilled pyrrole was stored at lower than 5°C temperature in the absence of light. All other chemicals were analytical grade.

2.2. Preparation of PPy

1.727 mL pyrrole was dissolved in 50 mL of de-ionized water and stirred for 15 min using a magnetic stirrer. 2.717 mL dilute H_2SO_4 was added slowly using dropper to the pyrrole monomer solution. 2.28 g ammonium persulphate (APS) was dissolved in 50 mL of deionised water and slowly added drop by drop from a burette to the above-prepared solution with constant stirring for half an hour. After stirring for 4 h, the solution was filtered, and the residue was washed with double distilled water, methanol, and acetone, and dried in oven at 60°C. Subsequently, the product was grinded to get powder of PPy [38].

2.3. Preparation of graphene oxide

GO was synthesized from graphite powder using a modified Hummer's method. In brief, first, 0.5 g of powdered flake of graphite and 0.5 g of $NaNO_3$ were added into 24 mL of H_2SO_4 and were stirred until dissolved. Then, 3 g of $KMnO_4$ was added slowly, preventing the temperature of the suspension from exceeding 20°C. After continuous stirring, the

mixture for 1 h at 35°C, 40 mL of distilled water was slowly added to dilute the mixture, and the temperature was raised to 90°C. To reduce the residual permanganate and manganese dioxide to colourless soluble manganese sulphate, 5 mL of 34.5% H_2O_2 was added, and the suspension was filtered with distilled water until pH 7.0. The obtained yellow-brown suspension was exfoliated to produce single-layer GO using a sonicator, and the unexfoliated precipitation was removed by centrifugation. Finally, we obtained a brown-black dispersion of homogeneously exfoliated GO [39].

2.4. Preparation of TiO₂/PPy nanocomposites

TiO₂ NPs, with an average particle size of 50 nm, were prepared by previously reported method [40]. 3.454 mL pyrrole and 5.434 mL dilute H_2SO_4 were stirred with 100 mL double-distilled water and 1.036 g TiO₂ added in the pyrrole reaction medium. 4.56 g APS was dissolved in 100 mL of deionized water and slowly added drop by drop from a burette to the above-prepared solution for half an hour. After stirring for 4 h, the solution was filtered, and the residue was washed with double distilled water, methanol, and acetone, dried in an oven at 60°C and grinded into powder [41].

2.5. Preparation of TiO₂/PPy/GO nanocomposites

3.454 mL pyrrole and 5.434 mL dilute H_2SO_4 were stirred with double-distilled water. 1.0362 g TiO₂ and 60 mg GO was added in the pyrrole reaction medium, and the mass ratio of TiO₂:PPY:GO was maintained at 8:17.5:1. The amount of 4.56 g APS was dissolved in 100 mL of deionized water and slowly added drop by drop using burette to the above-prepared solution for half an hour. After stirring for 4 h, the solution was filtered, and the residue was washed with double-distilled water, methanol, and acetone, dried in an oven at 90°C and grinded into powder [42].

2.6. Characterizations

The phase and purity of as-synthesized TiO₂, PPy, TiO₂/PPy, and TiO₂/PPy/GO materials were determined by X-ray diffraction (XRD) pattern recorded on analytical X'Pert Pro X-ray diffractometer in the 2θ range 10°–80° with the step size of 0.025°. The particle size of TiO₂ and morphology of particles was investigated with transmission electron microscope (TEM) images observed on JEOL JEM 200 CX equipment. The morphology of neat TiO₂, PPy, and TiO₂/PPy nanocomposites was investigated by scanning electron microscopy images recorded on JEOL 6490 LB equipment. The surface area and pore characteristics of the derived photocatalyst were determined by nitrogen adsorption/desorption isotherms at 77 K (boiling point of nitrogen gas at 1 atm pressure) using a Brunauer–Emmett–Teller (BET) surface area analyzer (BELSORP-max, Japan). The diffused reflectance spectroscopy study was done on Carry 100 spectrophotometer, and graphs were used to determine band gap energy of prepared nanocomposites. Photoluminescence (PL) spectra (recorded on Perkin Elmer LS 55 spectrofluorometer) were used to study emission behaviour and e^-–h^+ recombination determination of the samples.

2.7. Determination of the point of zero charge of powdered titania nanocomposites

The point of zero charge (PZC) of the titania nanocomposites was determined to employ the solid addition method using 0.1 mol L⁻¹ KCl and 0.002 mol L⁻¹ citrimide (C19H42BrN) surfactant solutions. 50 mL of KCl and citrimide solution was taken in a 100-mL stoppered conical flask. The initial pH values of the solutions were roughly adjusted to be between 2 and 12 by adding either 0.1 mol L⁻¹ HCl or 0.1 mol L⁻¹ NaOH. The initial pH of the solution was then accurately recorded. 1 g of the prepared titania-based nanomaterials was added to each flask. The suspensions were shaken and allowed to equilibrate with intermittent shaking. The final pH of the supernatant liquid was recorded. The difference between the initial and final pH values (pH = pH_i − pH_f) was plotted against the initial pH value. The point of intersection of the resulting curve where the change in pH is zero gives the value of the PZC [43].

2.8. Irradiation procedure

The solutions of dyes were prepared in 10:1 (V/V) ratio of water and alcohol. The known amount of photocatalyst was dispersed in the dye solution (20 mL). The desired concentrations of Victoria Blue and Rose Bengal dye (20 mL) were taken in a 100-mL beaker and 1 g of each photocatalyst, TiO₂, PPy, TiO₂/PPy, and TiO₂/PPy/GO, were mixed to dye solutions, and resulting suspensions were stirred on the magnetic stirrer in dark for 30 min to reach adsorption equilibrium. The visible light was irradiation was done by putting xenon lamp (1,000 W) vertically on the surface of the reaction medium with constant stirring. After desired time interval, an aliquot of the solution was isolated, centrifuged, and filtered through a Millipore filter to separate the photocatalysts, and their UV-Vis absorption spectra were recorded to determine the residual concentration.

The percentage of degradation efficiency of the samples was calculated using Eq. (1) [44,45]:

$$\eta\% = \frac{A_0 - A_F}{A_0} \times 100 \tag{1}$$

where h is the degradation efficiency; A_0 is the initial absorbance; and A_F is the final absorbance.

3. Results and discussion

3.1. X-ray diffraction patterns of nanocomposites

XRD patterns of pure TiO₂, PPy, TiO₂/PPy, and the TiO₂/PPy/GO synthesized nanocomposites are presented in Fig. 2. In the case of pure TiO₂ NPs, the main diffraction peaks observed at 25°, 38°, 48°, 55.1°, and 63.2° are (101), (103), (200), (211), and (204), respectively, planes of TiO₂ (JCPDS file No: 86-1157; Fig. 2(a)). In the XRD pattern of GO obtained via the improved Hummers' method, the (0 0 1) crystal plane of GO was observed, with a spacing of 8.33 Å, which is typical for GO. In the XRD pattern of pure PPy (Fig. 2(b)), the observance of a broad peak in the 2θ region 20°–50° revealed that the as-synthesized PPy is amorphous in absence of TiO₂. Broad peaks in the region 15° < 2θ < 30° are revealing that the resulting PPy powders are amorphous in nature. This agrees well with the structure reported in literature [16]. Such broad
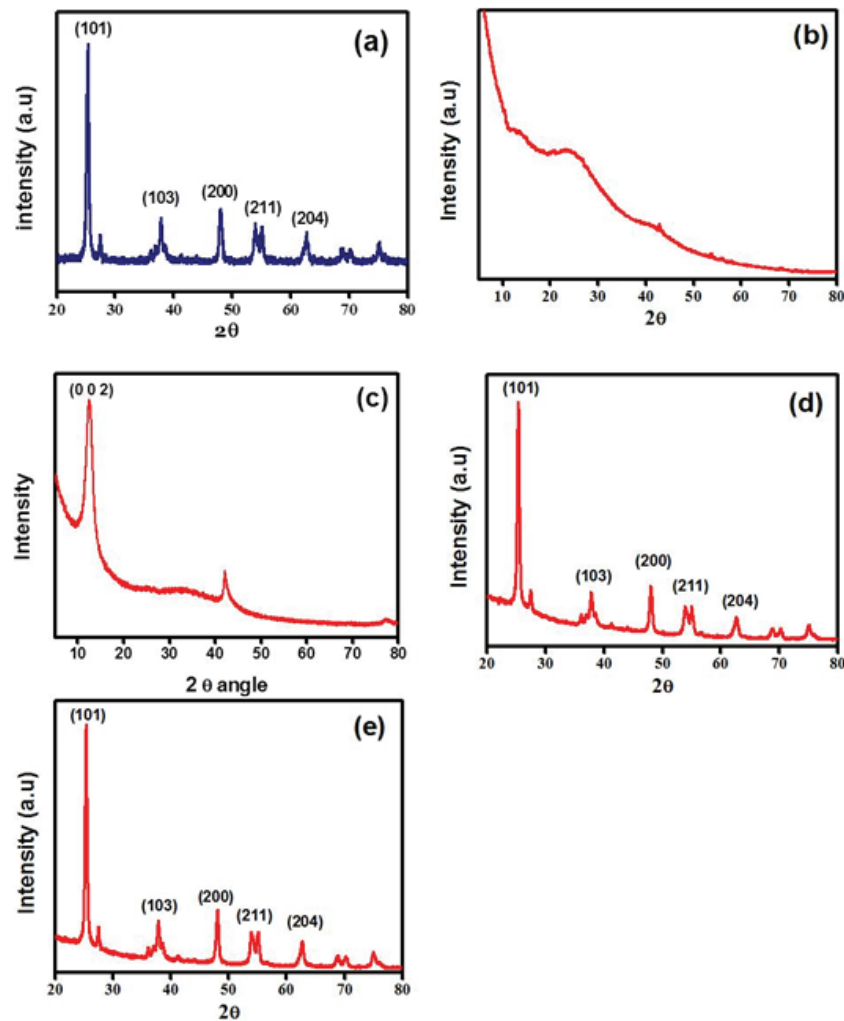
Fig. 2. XRD of: (a) TiO_2, (b) pure PPy, (c) pure GO, (d) TiO_2/PPy, and (e) TiO_2/PPy/GO.

peak usually indicates short-range arrangement of chains. It can be seen from Figs. 2(c) and (d) that the main peaks of TiO_2/PPy and TiO_2/PPy/GO nanocomposites are similar to those of neat TiO_2 NPs but broad weak diffraction peak of PPy still exists; however, its intensity has been decreased. It implies that when pyrrole is polymerized on TiO_2; each phase maintains its initial structure [46,47].

3.2. Determination of average size of particles/grains in samples

Utilizing the observed XRD data of samples, Scherrer's calculations were attempted to know the average size of crystal in the samples [48]. Although Scherrer's calculations are only approximate in nature, but definitely provide a first-hand idea of the average size of the crystal in the samples, which may be quite accurate, provided the size of crystal is below 100 nm.

$$B = \frac{0.9\lambda}{t \cos\theta} \qquad (2)$$

The mean size of TiO_2, TiO_2/PPy, and TiO_2/PPy/GO nanocomposites, calculated by Scherrer's equation, are about 19, 24, and 30 nm, respectively. The results of Scherrer's calculations are presented in Table 2. The results suggest average size of the crystal in the samples lying in nm range.

The morphology and shape of pure TiO_2 NPs, neat PPy, TiO_2/PPy, and TiO_2/PPy/GO nanocomposites were characterized by scanning electron microscope (SEM) instrument, and the obtained pictures are presented in Fig. 3. As shown in Fig. 3(b), TiO_2 NPs were aggregated due to their high surface energy. In the corresponding TEM image (Fig. 4(a)), 30 ± 10 nm diameter polygonal prism-like structures have been observed. In the SEM image (Fig. 3(a)) and TEM image (Fig. 4(b)), cloud-like image of pure PPy has been observed. The SEM and TEM images (Figs. 3(c) and 4(c)) show that the morphology of TiO_2/PPy composite is similar to pure PPy. In the SEM image (Fig. 3(d)), aggregates of TiO_2/PPy/GO were observed; however, in the TEM image (Fig. 4(d)), multi-facet polygonal prismatic structures, with diameter 40 ± 15 nm, have been observed. Above data indicate that PPy polymerizes in the presence of
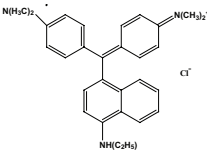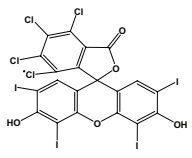
Table 1
Showing the structure and properties of dyes

Dye	Victoria Blue	Rose Bengal
Structure		
Molar mass:	$[C_{33}H_{40}N_3]Cl$, 507.5 g/mol	$C_{20}H_4Cl_4I_4O_5$, 973.67 g/mol
λ_{max}	614 nm	547 nm

Table 2
Average size of crystal in the samples of TiO_2 and TiO_2, TiO_2/PPy, and $TiO_2/PPy/GO$

Sample	Particle size (nm)
TiO_2	19
TiO_2/PPy	24
$TiO_2/PPy/GO$	30

GO. The SEM images help us draw a conclusion that the doping of TiO_2 has no effect on PPy's morphology; however, presence of TiO_2 along with GO retains the similar structure for $TiO_2/PPy/GO$ as observed in case of pure TiO_2 [24].

3.3. Bruner–Ernst–Teller Surface area analysis

Nitrogen adsorption–desorption isotherms were used to determine the structural characteristics and surface area of TiO_2, TiO_2/PPy, and $TiO_2/PPy/GO$ nanocomposite. The N_2 adsorption–desorption isotherms of the TiO_2, TiO_2/PPy, and $TiO_2/PPy/GO$ nanocomposite were measured at 77 K, as shown in Fig. 5. The specific surface areas from BET and surface area, pore volume, and pore radius of the TiO_2, TiO_2/PPy, and $TiO_2/PPy/GO$ nanocomposite are shown in Table 3. The surface area was found 37.52, 76.68, and 96.24 m²/g for TiO_2, TiO_2/PPy, and $TiO_2/PPy/GO$, respectively. There is an increase in V_p and pore radius of the TiO_2, TiO_2/PPy, and $TiO_2/PPy/GO$ nanocomposite [49]. From these results, it may be concluded that the high surface area of the $TiO_2/PPy/GO$ nanocomposite may favour rapid electron transport and high ion diffusion, allowing improved photochemical performance. Moreover, the BET surface areas increased remarkably in the $TiO_2/PPy/GO$ nanocomposite, which suggests that TiO_2 is well intercalated in PPy matrix and may also provide direct conduction
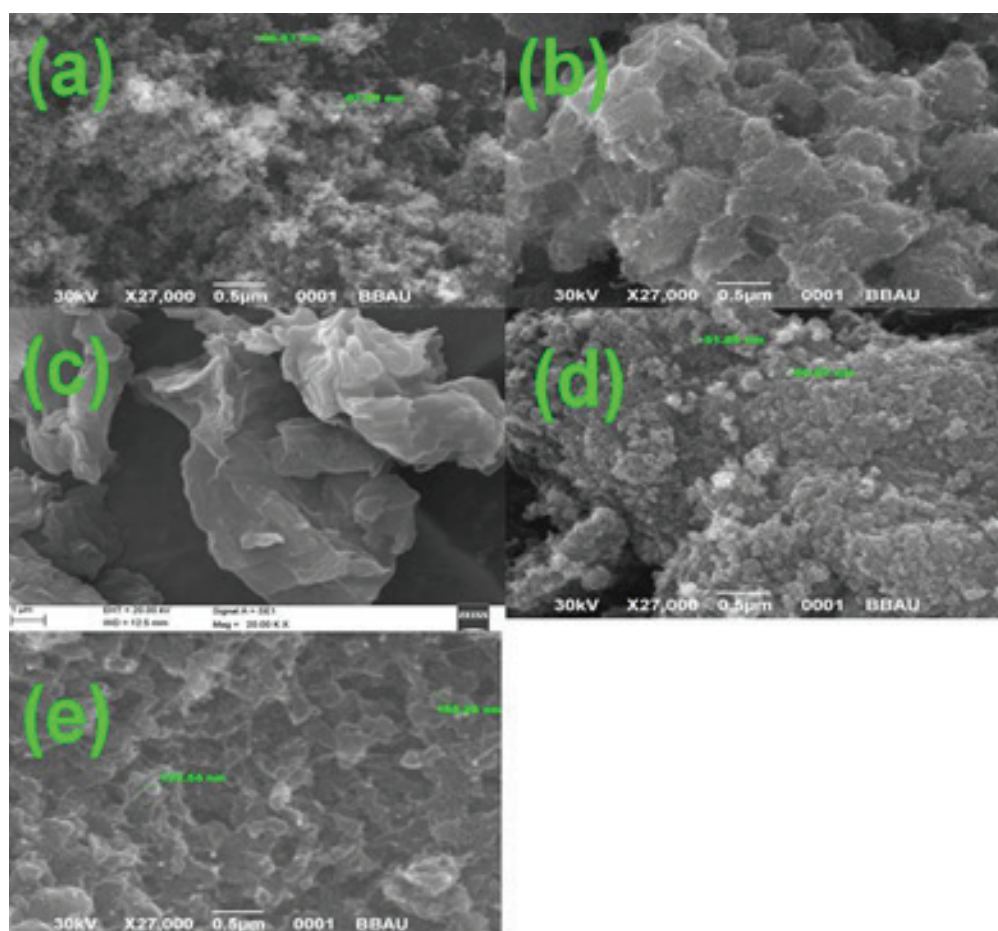

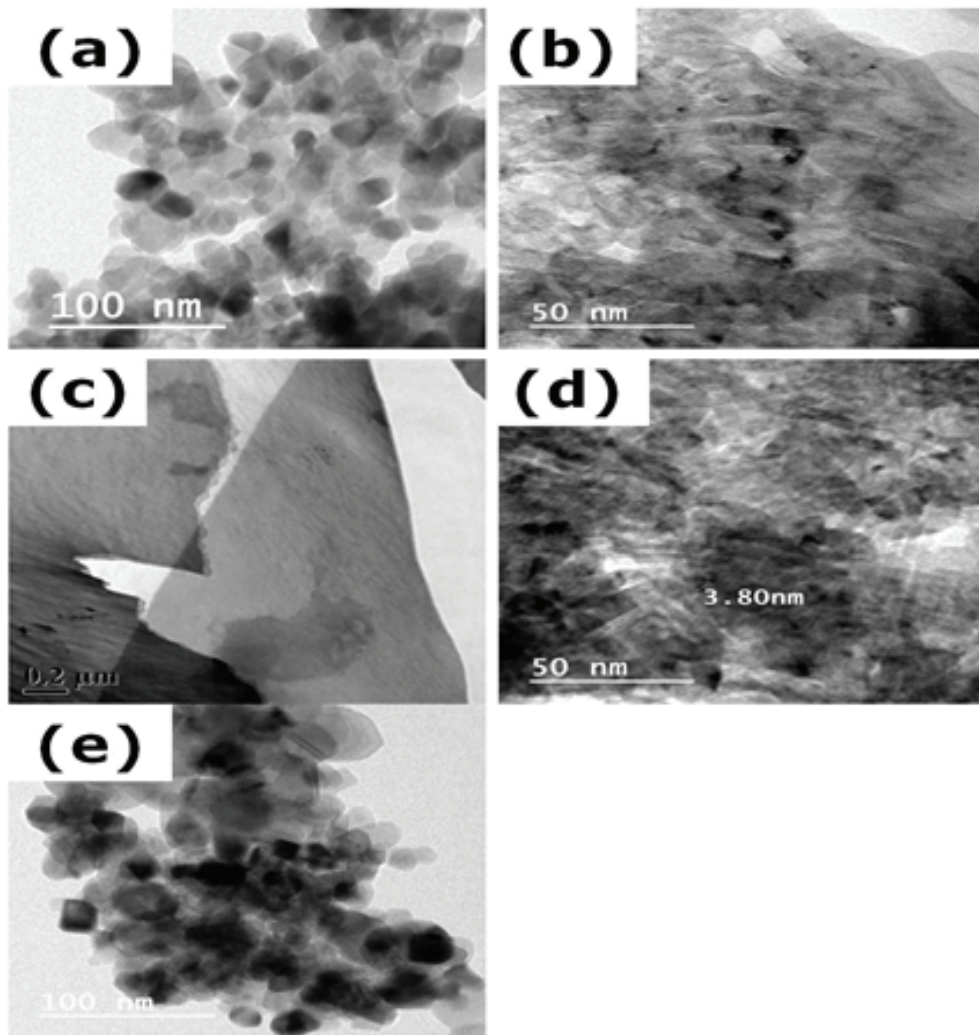Fig. 3. SEM images of: (a) TiO_2, (b) pure PPy, (c) pure GO, (d) TiO_2/PPy, and (e) $TiO_2/PPy/GO$ nanocomposites.

Fig. 4. TEM of: (a) TiO$_2$, (b) pure PPy, (c) GO, (d) TiO$_2$/PPy, and (e) TiO$_2$/PPy/GO.

pathway for electrons. The formation of TiO$_2$ with PPy by co-deposition oxidation synthesis resulted in the generation of well-dispersed TiO$_2$ in PPy matrix giving one TiO$_2$/PPy system with unique set of properties [50].

3.4. UV-Visible spectra of nanocomposites

The prepared nanocomposites aqueous suspensions were used for the UV absorption studies. The absorption spectrum of TiO$_2$ consists of a single, broad intense absorption between 250 and 400 nm due to the charge-transfer from the valence band to the conduction band (CB) [51]. The TiO$_2$ showed absorbance in the shorter wavelength region while PPY, GO, TiO$_2$/PPy, and PPy/ TiO$_2$/GO result showed slight redshift in the absorption edge. The absorption spectrum of TiO$_2$ consists of a single, broad intense absorption around 383 nm (shown in Fig. 6) in the region of the hypsochromic shift. The TiO$_2$/PPy results showed a redshift in the absorption onset value, and the broad peak observed at 410 nm. This is due to the coating of PPy layer on the surface of titania [52]. The redshift that is observed at 410 nm in the absorption spectra with the decrease in particle size has been reported in

TiO$_2$/PPy/GO nanocomposite. This is due to the coating of PPy and GO in the titania and the titania completely interacted with PPy and GO.

3.5. Determination of optical band gap of nanocomposites

The UV-Visible (UV-Vis) spectra of the titania-based nanocomposites have been recorded, and the data were used to determine band gap values. The band gap of materials was determined by the Tauc relation (Eq. (3)):

$$\alpha h\nu = B(h\nu - E_{gap})^m \tag{3}$$

where α is the absorption coefficient; hν is the photon energy; and $m = \frac{1}{2}$ for direct band gap material shown in Fig. 7. To describe a direct method for fitting and determination of band gap using Tauc relation [51,52], we can rewrite Eq. (3) as:

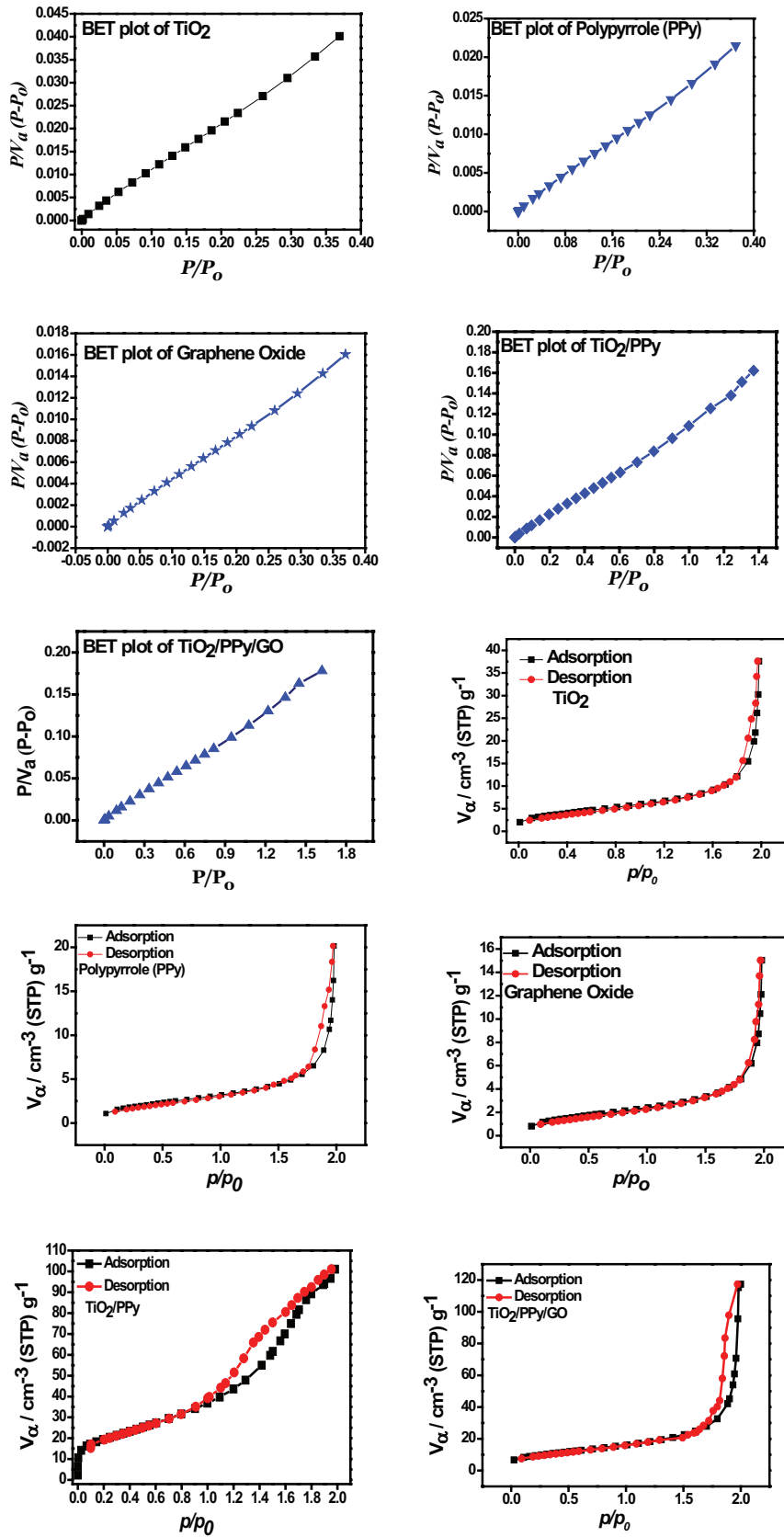$$\left(\frac{Abs}{\lambda}\right)^{1/m} = B\left(\frac{1}{\lambda} - \frac{1}{\lambda_{gap}}\right) \tag{4}$$

Fig. 5. BET and adsorption–desorption plot for TiO$_2$, PPY, GO, TiO$_2$/PPy, and PPy/ TiO$_2$/GO.

Table 3
The specific surface area, pore volume, and pore radius of the TiO$_2$, TiO$_2$/PPy and PPy/ TiO$_2$/GO

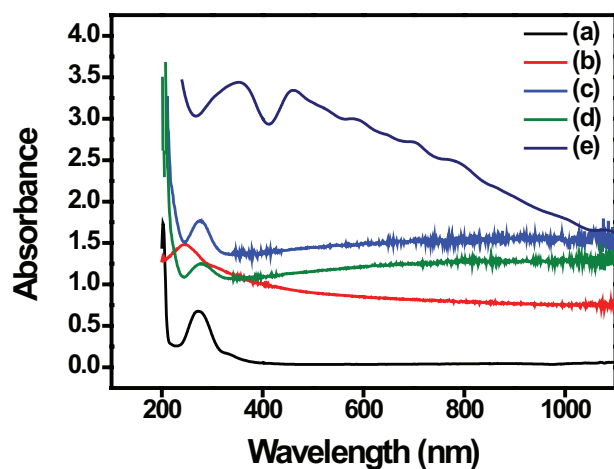| Sample	Surface area (m^2/g)	Pore volume (cm^2/g)	Pore radius (nm)
TiO$_2$	37.52	3.132	1.21
PPy	19.83	2.632	1.12
GO	14.86	2.142	1.02
TiO$_2$/PPy	76.68	6.5124	1.64
TiO$_2$/PPy/GO	96.24	9.5124	1.84

Fig. 6. UV-Visible spectra of nanocomposites: (a) TiO$_2$, (b) PPy, (c) GO, (d) TiO$_2$, and (e) TiO$_2$/PPy/GO.

where λ is the wavelength; Abs, the corresponding value of measured absorbance; λ_{gap} can be easily obtained from curve $(Abs/\lambda)^{1/m}$ vs. $1/\lambda$ plot at condition $(Abs/\lambda)^{1/m} = 0$. The band gap value is obtained from relation $E_{gap} = 1{,}239.83/\lambda_{gap}$. The band gap of samples was calculated by extrapolation of the $(\alpha hn)^2$ vs. hn plots, where α is the absorption coefficient and hn is the photon energy; $hn = (1{,}239/\lambda)$ eV. The value of hn extrapolated to $\alpha = 0$ gives an absorption energy, which is correspond to a band gap (E_{gap}). Fig. 7 yields an E_{gap} value of 3.2 eV for TiO$_2$, 2.98 eV for pure PPy, 2.65 eV for TiO$_2$/PPy, and 2.45 eV for TiO$_2$/PPy/GO [53]. The band gap values of nanocomposites slightly decrease compared with pure TiO$_2$ because the electrons of pure PPy are excited from the HOMO to the LUMO of PPy whereas holes were left in the HOMO of PPy. The excited-state electrons can be readily injected into the CB of TiO$_2$ [54].

3.6. Determination of point of zero charge of nanocomposites

The PZC of the titania nanocomposites was determined employing the solid addition method. The PZC was found 6.4, 6.6, and 6.9 for the TiO$_2$, TiO$_2$/PPy, and TiO$_2$/PPy/GO. It is shown in Fig. 8.

3.7. Photodegradation

3.7.1. Effect of pH

The photodegradation of dyes are affected by the pH of the solution. The variation of solution pH changes the surface charge of TiO$_2$ particles and shifts the potentials of catalytic reactions. As a result, the adsorption of dye on the surface is altered thereby causing a change in the reaction rate. Titania has PZC at 6.9. Under acidic or alkaline condition,
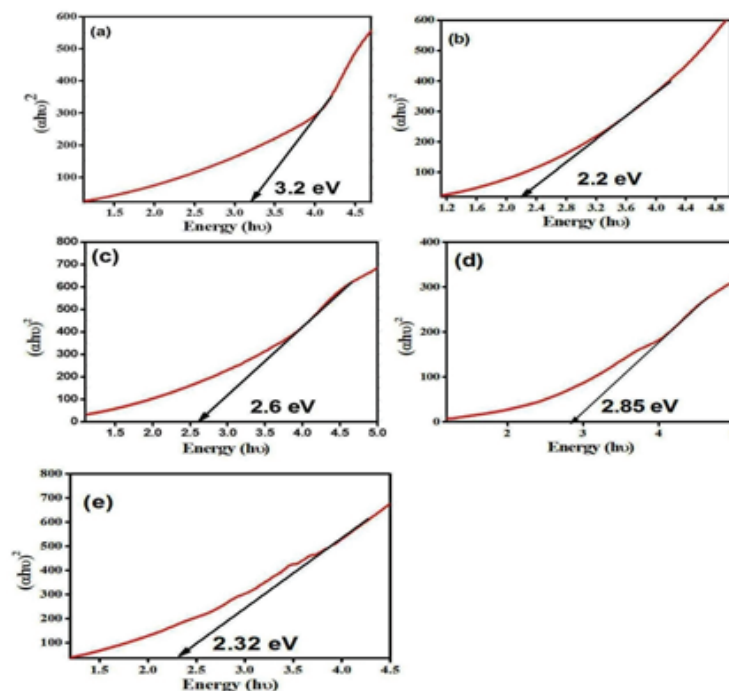

Fig. 7. Band gap energy of: (a) pure TiO$_2$, (b) pure PPy, (c) GO, (d) TiO$_2$/PPy, and (e) TiO$_2$/PPy/GO. nanocomposites.

the surface of titania can be protonated or deprotonated according to the following reactions [55]:

$$TiOH + H^+ \rightarrow TiOH_2^+ \tag{5}$$

$$TiOH + OH^- \rightarrow TiO^- + H_2O \tag{6}$$

Thus, titania surface will remain positively charged in acidic medium (pH < 6.9) and negatively charged in alkaline medium (pH > 6.9). TiO_2 is reported to have higher oxidizing activity at lower pH, but excess H^+ can decrease reaction rate. TiO_2 behaves as a strong Lewis acid due to the surface positive charge. In other words, the anionic dye acts as a strong Lewis base and can easily adsorb on the positively charged catalyst surface. This favours the adsorption of the dye under acidic conditions, while in the alkaline conditions this complexation process is not favoured presumably because of competitive adsorption by hydroxyl groups and the dye molecule in addition to the Coulombic repulsion due to the negatively charged catalyst with the dye molecule [56]. The extent of dye adsorption depends on the initial dye concentration, nature of the dye, surface area of photocatalyst, and pH of the solution. The pH determines the surface charge of the photocatalyst. Adsorption of the dye is minimum when the pH of the solution is at the isoelectric point (PZC) [43]. The surface of the photocatalyst is positively charged below isoelectric point and carries a negative charge above it.

Bubacz et al. [57] observed an increase in the rate of the photocatalytic degradation of methylene blue with an increase in pH. According to Ling et al. [58], basic pH electrostatic interactions between negative TiO^-, and methylene blue cation lead to strong adsorption with a correspondingly high rate of degradation. The surface charge properties of TiO_2 were also found to be changed with a change of pH value due to the amphoteric behaviour of semiconducting TiO_2 [59–62] and also found that the degradation of Reactive Black 5 and Reactive Orange 4 dyes was favoured in acidic medium with
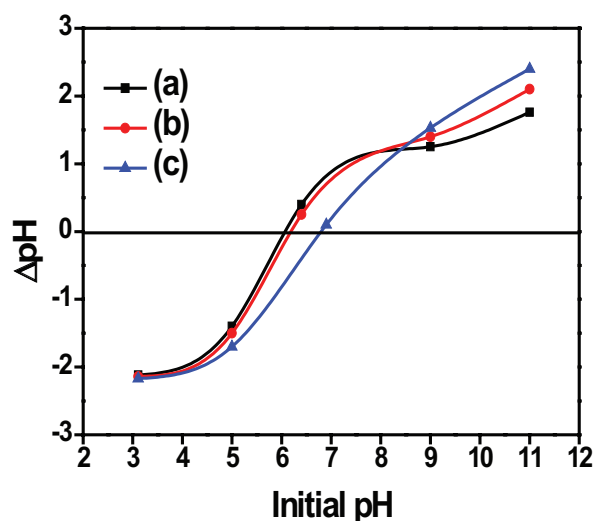
TiO_2. Tanaka et al. [63] found that positively charged TiO_2 surface adsorbed more Acid Orange 7 at lower pH value, and more decomposition was achieved. The acid black 1 has a sulphuric group in its structure, which is negatively charged. Therefore, the acidic solution favours adsorption of dye onto photocatalyst surface as TiO_2 surface is positively charged in acidic solution [64].

The photodegradation of cationic dyes (Victoria Blue) and anionic dye (Rose Bengal) was carried out under varying pH conditions from 2 to 9, by the addition of H_2SO_4 and NaOH, keeping other parameters constant (concentration = 50 ppm, the amount of catalysts = 800 mg/L, and irradiation time = 120 min). The results show that degradation of dye Victoria Blue is highest in basic medium (at pH = 10) shown in Fig. 9. Under acidic conditions, it was found difficult to adsorb the cationic VB dye onto the TiO_2 surface. The active •OH radicals formed in low concentrations, and hence, the photodegradation process of VB remained slow. With higher pH values, the formation of active •OH species is favoured, due to not only improved transfer of holes to the adsorbed hydroxyls but also electrostatic abstractive effects between the negatively charged TiO_2 particles and the operating
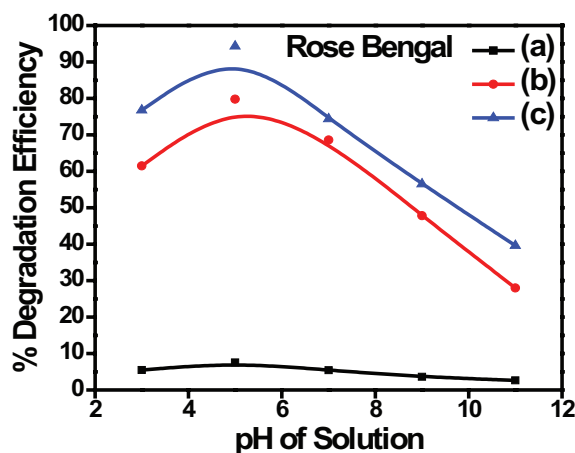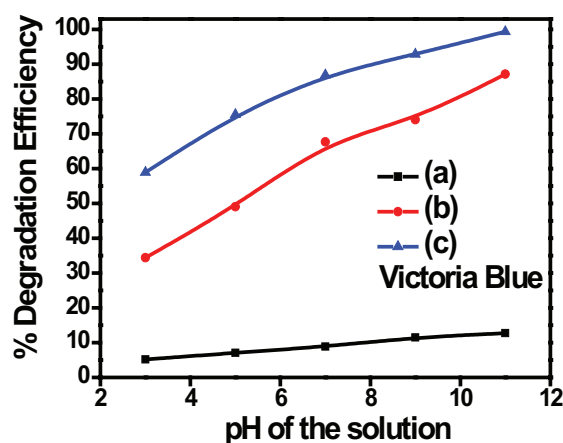

Fig. 8. Determination of PZC of nanocomposites: (a) TiO_2, (b) TiO_2/PPy, and (c) TiO_2/PPy/GO.

Fig. 9. Effect of pH on photodegradation efficiency of dyes Victoria Blue and Rose Bengal: (a) TiO_2, (b) TiO_2/PPy, and (c) TiO_2/PPy/GO.

cationic dyes. Although the VB dye can adsorb onto the TiO_2 surface to some extent in alkaline media, when the pH value is too high (pH 11), the VB dye molecules will change to a leuco compound. Our results indicate that the TiO_2 surface is negatively charged, and the VB adsorbs onto the TiO_2 surface through the positive ammonium groups. This is characteristic of heterogeneous photocatalysts, and the results are in agreement with the earlier studies [65].

The photodegradation of Rose Bengal is highest in acidic medium at pH 5 shown in Fig. 9. This implies that the acidic condition is favourable for the formation of the reactive intermediate hydroxyl radicals for Rose Bengal. This further helps in enhancing the reaction rate. On the other hand, in the neutral condition, the formation of reactive intermediate is relatively less favourable and hence not feasible [66]. The rate of photodegradation increases with increases in pH of the solution. At lower pH (3) values, the surface of catalyst is negatively charged, and the dye molecules are positively charged. Therefore, the dye molecules and catalyst particles will attract each other. Thus, catalytic reaction on the surface of TiO_2 will take place to a greater extent. However, it is reported to have higher oxidizing activity at lower pH, but excess H^+ can decrease reaction rate of photodegradation of dye. But the maximum photodegradation of Rose Bengal dye was found at pH 5; this is because that decrease in H^+ concentration and adsorption of Rose Bengal (anionic dye) is higher at pH 5, because the force of attraction between catalyst surface and dye molecules will start operating, thus resulting in increase in rate of dye degradation [67].

3.7.2. Effect of photocatalyst and dose

The effect of photocatalysts and their doses on the degradation of dyes Victoria Blue and Rose Bengal is shown in Figs. 10 and 11. It is clear from the results that the TiO_2, TiO_2/PPy, and $TiO_2/PPy/GO$ are effective photocatalyst for degradation of Victoria Blue and Rose Bengal dye; however, $TiO_2/PPy/GO$ seems to be the most effective photocatalyst for degradation of Victoria Blue and Rose Bengal. Further photodegradation efficiency of the catalysts follows the trend $TiO_2 < TiO_2/PPy < TiO_2/PPy/GO$. The effect of photocatalyst dose on the photodegradation of Victoria Blue and Rose

Bengal was studied by applying different concentrations (from 50 to 800 mg/L) of the photocatalyst is shown in Fig. 11. Initially (from 50 to 200mg/L), the rate of degradation of the dyes Victoria Blue and Rose Bengal was very rapid; after that, it became slow and attained plateau at 800 mg/L due to occupancy of all active sites at this concentration. When the PPy is coated in TiO_2, the band gap energy is decreased which enhanced the photoefficiency, the surface area of photocatalyst also increased the photoefficiency of the photocatalyst.

3.7.3. Effect of dye concentration

The effect of dyes concentration on photocatalytic degradation was studied in presence of TiO_2, TiO_2/PPy, and $TiO_2/PPy/GO$ nanocomposites materials, keeping the amount of catalyst constant. A known concentration of dye solution was prepared in water: alcohol 10:1 (V:V) ratio. The 800 mg/L of photocatalyst was dispersed in the different concentration of dye solution (20, 40, 60, 80, and 100 ppm for Victoria Blue and 25, 50, 75, 100, and 125 ppm Rose Bengal), and the reaction mixture was irradiated by visible light. The effect of photocatalytic degradation with time was measured, and the results are shown in Fig. 12. The highest photodegradation efficiency (97%) of both dyes was found in the presence of $TiO_2/PPy/GO$ nanocomposite while in presence of TiO_2/PPy and neat TiO_2, it was 86% and 16%, respectively. When the concentration of solution increased, the number of dye molecule also increased; therefore, the effective number of photon penetrating the dye reached at the catalyst surface also reduced, owing to hindrance in the path of light, thereby reducing the reactive hydroxyl and superoxide radicals and decreasing the percentage of degradation [65–67].

3.7.8. GC-MS of VB and RB photodegradation products

The photodegradation of the Victoria Blue and Rose Bengal takes place by irradiating under visible light in the presence of TiO_2, TiO_2/PPy, and $TiO_2/PPy/GO$ nanocomposite. The photodegraded products of photodegradation of Victoria Blue and Rose Bengal have been determined by GC-MS (gas chromatography–mass spectrometry) analysis (Figs. 13 and 14). It has been found that MS chromatograph
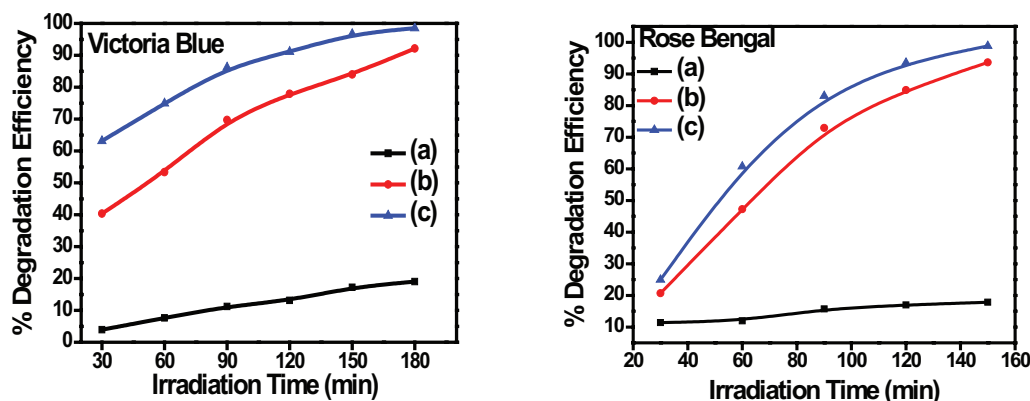

Fig. 10. Effect of irradiation time on photodegradation efficiency of dyes Victoria Blue and Rose Bengal: (a) TiO_2, (b) TiO_2/PPy, and (c) $TiO_2/PPy/GO$.
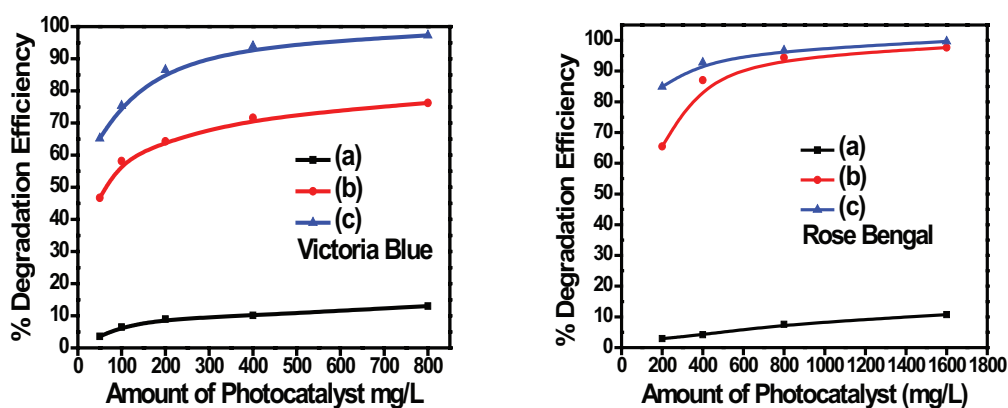
Fig. 11. Effect of photocatalyst amount on efficiency of dyes Victoria Blue and Rose Bengal: (a) TiO$_2$, (b) TiO$_2$/PPy, and (c) TiO$_2$/PPy/GO.
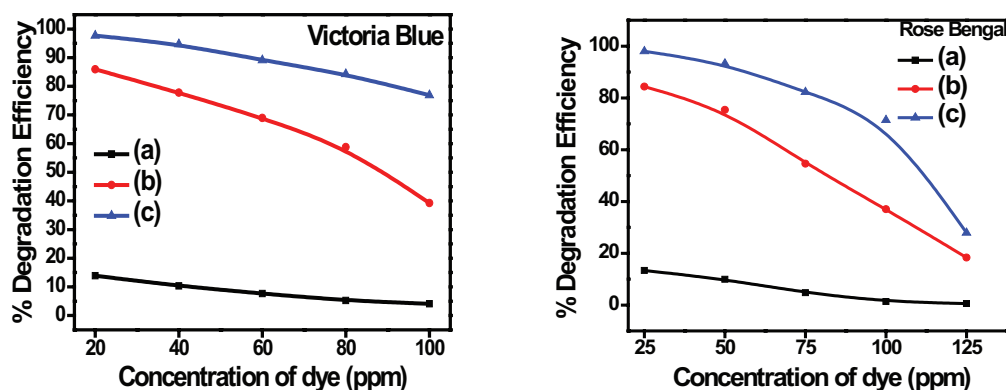

Fig. 12. Effect of concentration on photodegradation efficiency of dyes Victoria Blue and Rose Bengal: (a) TiO$_2$, (b) TiO$_2$/PPy, and (c) TiO$_2$/PPy/GO.

(Figs. 15 and 16) and correspondingly mass chromatographs of Victoria Blue and Rose Bengal (after 2 h of irradiation) in the presence of TiO$_2$, TiO$_2$/PPy, and TiO$_2$/PPy/GO are almost similar, except in their respective intensities (Figs. 15 and 16). Among the number of degraded products of Victoria Blue and Rose Bengal, seven products formed in the photodegradation, shown in mass chromatograph (Figs. 15 and 16), have been identified, as listed in Table 4.

The mechanism for the photodegradation of Victoria Blue and Rose Bengal using titania nanocomposites is believed to take place by the photo produced e$^-$ and h$^+$ that results into formation of highly oxidative species such as hydroxyl and superoxide radicals, which on reaction with Victoria Blue and Rose Bengal results into its decomposition to smaller molecules [68].

The mass spectroscopy has been studied to identify the possible reaction intermediates after 180 min of reaction, as shown in Fig. 17. The RB dye solution displays a prominent mass signal at m/z = 1,022 in Fig. 13, that is, very close to the formula mass of RB dye. Noticeably, no mass signals are detected about the formation of the reaction intermediates, which clearly reveal the removal by adsorption. The m/z = 1,022 signal is weakened after 180 min of photocatalytic reaction over the TiO$_2$/PPy/GO nanocomposites, and multiple mass signals have appeared (Fig. 17 indicates the

formation of reaction intermediates during the photocatalytic degradation). Fig. 17 depicts the molecular structures of possible reaction intermediates from fragmentations of the main skeleton of RB dye, which have the oxy groups in their rings. It is believed that the formations of these reaction intermediates are crucial to determine the degree of degradation of the organic compounds to complete mineralization [69].

3.8. Recyclability of photocatalyst

In order to observe reusability, the photocatalyst recyclability has been studied in this work. The photocatalyst and Victoria Blue and Rose Bengal mixture was agitated and illuminated with visible light, and after desired time, the mixture was centrifuged to remove the photocatalyst. The obtained photocatalysts were washed 3 times with distilled water and finally kept in oven for 24 h at 60°C temperature, and further, it is reused for the degradation of dyes. The photodegradation of Victoria Blue and Rose Bengal by the recyclized photocatalyst are shown in Figs. 18 and 19, respectively. The results show that the recyclized photocatalyst efficiency is decreased due to the loss of some active sites and decrease of collection efficiency of photon [70].
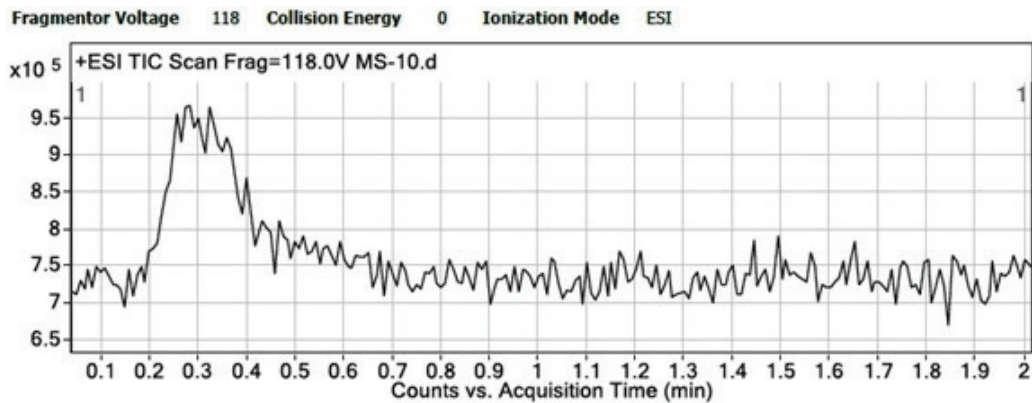
Fig. 13. GC chromatogram of Victoria Blue dye in presence of TiO_2/PPy/GO.

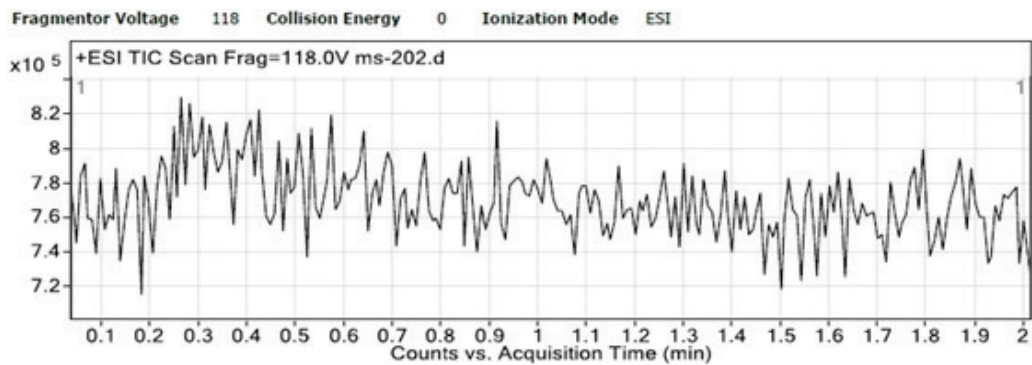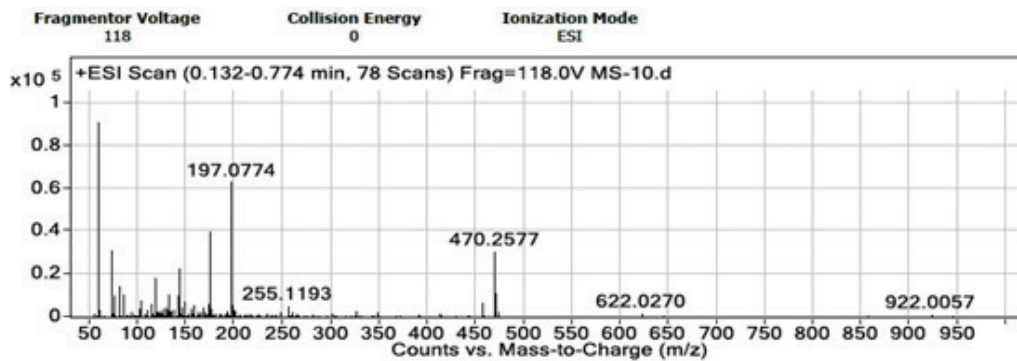Fig. 14. GC chromatogram of Rose Bengal dye in presence of TiO_2/PPy/GO.

Fig. 15. Mass chromatogram of Victoria Blue dye in presence of TiO_2/PPy/GO.

3.9. Total organic carbon analysis of photodegraded dyes

In order to measure the complete mineralization of Victoria Blue and Rose Bengal dyes, a total organic carbon (TOC) analysis was performed. During the initial stage of recirculation in the dark (30 min), the chemisorptions of the dyes on the catalyst surface caused a TOC depletion of 5%–8%. The experimental data obtained by using either TiO_2 or TiO_2/PPy and TiO_2/PPy/GO are shown in Fig. 20. The blank test of dye (without photocatalyst) is also reported for comparison for photocatalytic activity of nanocomposites; a maximum decrease of the TOC percentage is observed in the presence of the TiO_2/PPy/GO nanocomposites [71].

The TOC analysis of photodegraded Victoria Blue and Rose Bengal dye in presence of TiO_2, TiO_2/PPy, and TiO_2/PPy/GO was done. The TOC of Victoria Blue is shown in Fig. 21. The Victoria Blue was photodegraded for 3 h in presence of photocatalyst. The TOC of Victoria Blue was observed 100%, 92%, 26%, and 4% for the blank, TiO_2, TiO_2/PPy, and TiO_2/PPy/GO, respectively. The PPy-modified titania material shows the good photocatalytic activity. Similarly, The TOC was observed for the Rose Bengal dye shown in Fig. 21. The TOC photodegraded Rose Bengal was found 100%, 94%, 34%, and 16% for blank, TiO_2, TiO_2/PPy, and TiO_2/PPy/GO, respectively. It means that PPy-modified
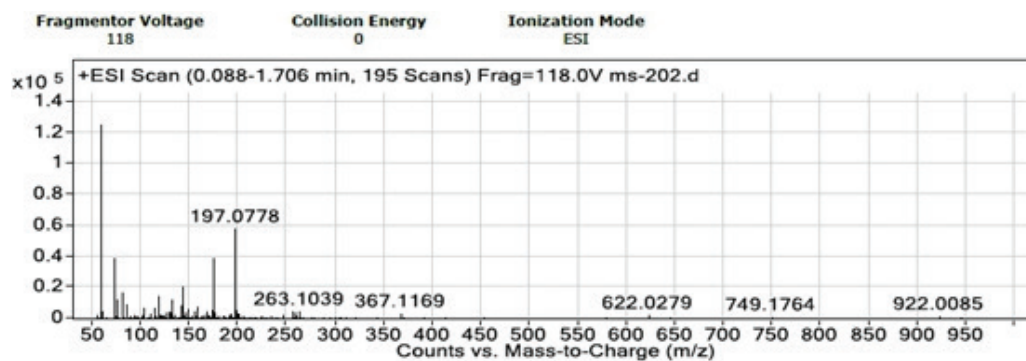
Fig. 16. Mass chromatogram of Rose Bengal dye in presence of TiO₂/PPy/GO.

Table 4
Different intermediate products form in the photodegradation of Victoria Blue dye

|	Compound	M + 1
[1]	(4-dimethylaminophenyl) (4-methylaminophenyl) (4-ethylaminonaphthyl)methylium	408, 392, 379, 258
[2]	(4-dimethylaminophenyl) (4-aminophenyl) (4-aminonaphthyl)methylium	366, 259, 244, 216
[3]	(4-hydroxymethylaminophenyl) (4-methylaminophenyl) (4-ethylaminonaphthyl)methylium	424, 395, 303, 275
[4]	(4-aminophenyl) (4-aminophenyl) (4-hydroxyethylaminonaphthyl)methylium	382, 260, 232
[5]	(4-hydroxymethylaminophenyl) (4-methylaminophenyl) (4-ethylaminonaphthyl)methylium	424, 303, 275,
[6]	(4-dimethylaminophenyl) (4-hydroxymethylaminophenyl) (4-ethylaminonaphthyl)methylium	424, 395, 317, 288
[7]	(4-aminophenyl) (4-aminophenyl) (4-ethylaminonaphthyl)methylium	36, 336, 273, 245
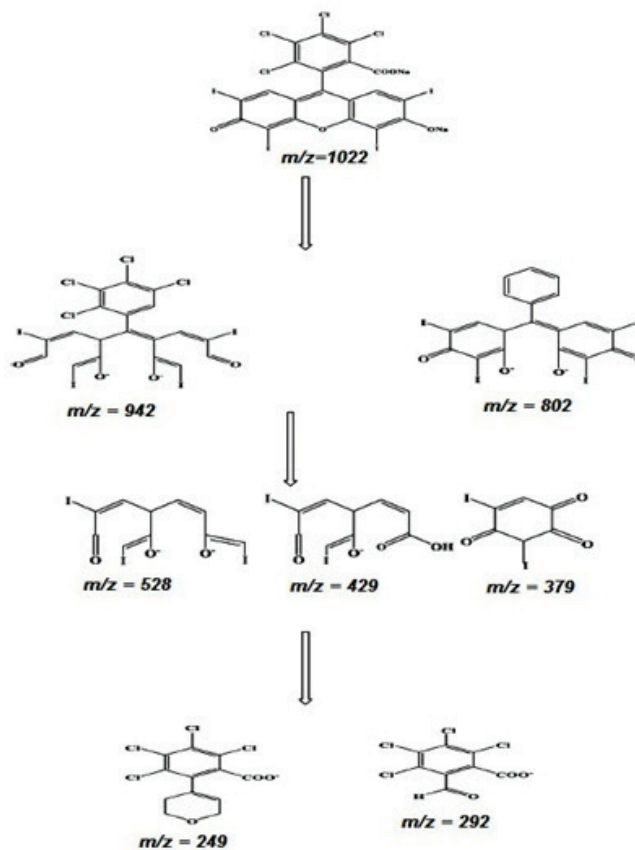
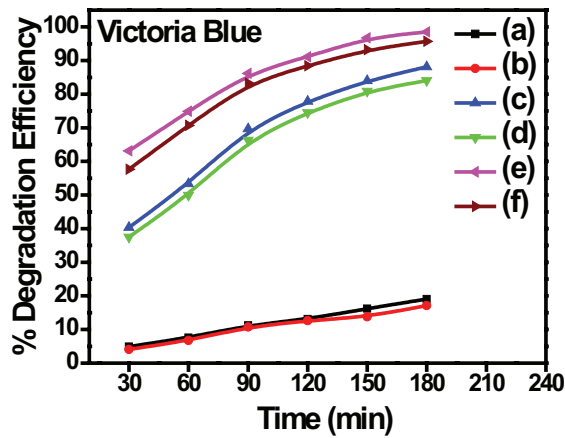Fig. 17. Photodegradation products of Rose Bengal dye identified by mass spectra.

Fig. 18. Photodegradation of Victoria Blue by photocatalyst and recyclable photocatalyst: (a) TiO_2, (b) recyclized TiO_2, (c) TiO_2/PPy, (d) recyclized TiO_2/PPy, (e) TiO_2/PPy/GO, and (f) Recyclized TiO_2/PPy/GO.

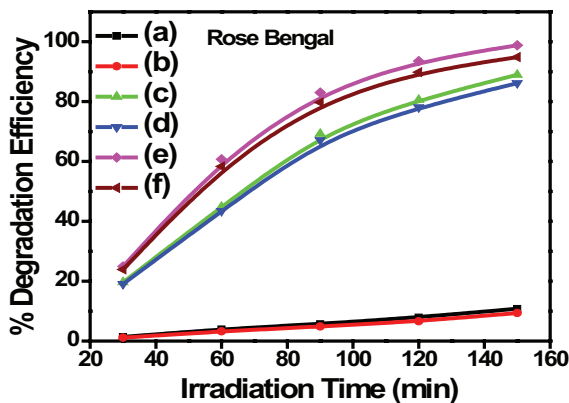Fig. 19. Photodegradation of Rose Bengal by photocatalyst and recyclable photocatalyst: (a) TiO_2, (b) recyclized TiO_2, (c) TiO_2/PPy, (d) recyclized TiO_2/PPy, (e) TiO_2/PPy/GO, and (f) recyclized TiO_2/PPy/GO.
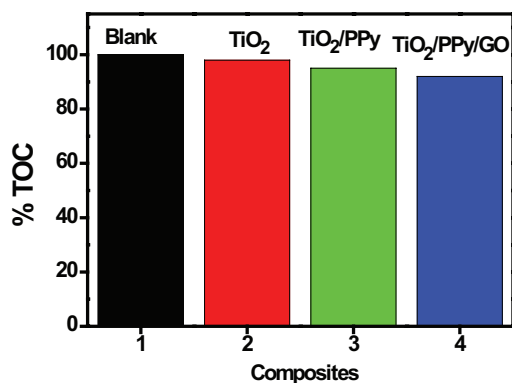

Fig. 20. Percentage of TOC of dye after adsorption (keep in under dark for 30 min).

titania shows the good photocatalytic activity due to formation of heterostructures [72].

3.10. Hydroxyl radical formation

To determine whether reactive oxygen species involved in the photocatalytic degradation of dyes is hydroxyl radical or not, terephthalic acid (TA) PL probing technique was used. In this method, alkaline solution of TA, having TiO_2, TiO_2/PPy, and TiO_2/PPy/GO nanocomposites was irradiated with visible light. After 30 min of irradiation, a sample was withdrawn from the reaction mixture and was centrifuged to separate photocatalyst particles. The PL spectrum of the sample was recorded between 335 and 600 nm at an excitation wavelength of 325 nm, and variation in the intensity of a peak at 425 nm was monitored using Perkin Elmer LS 55 Fluorescence Spectrometer.

As hydroxyl radical performs the key role in the decomposition of the organic pollutants, it is necessary to investigate a number of hydroxyl radicals produced by each photocatalyst. Thus, there is a technique to establish the formation of hydroxyl radicals using TA as a probe molecule. In this method, TA was directly attacked by •OH radical forming 2-hydroxyl TA (TAOH), which gives a fluorescence signal at 426 nm. Fig. 22 depicts the fluorescent signal of all the photocatalysts after reacting with TA solution. The fluorescent intensity is linearly related to the number of hydroxyl radicals formed by the photocatalysts. If the generation of hydroxyl radical is higher, the yield of TAOH will be more, and hence, more intense will be the fluorescence peak. Thus, TiO_2/PPy/GO
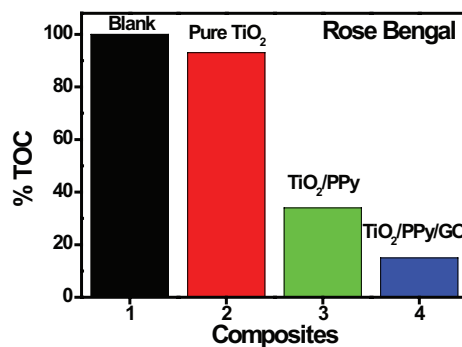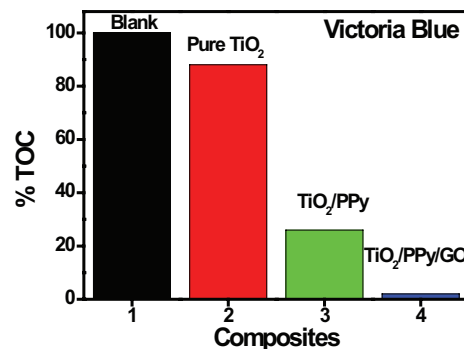

Fig. 21. Percentage of TOC of dyes after photodegradation with TiO_2, TiO_2/PPy, and TiO_2/PPy/GO.

with the highest intensity confirms the generation number of hydroxyl radicals compared with other photocatalysts. The fluorescence intensity follows the trend (i.e., $TiO_2 < TiO_2/PPy < TiO_2/PPy/GO$) of photocatalytic performance of all the photocatalyst [24].

3.11. Lowering of electron-hole recombination

PL spectra have been used to examine the mobility of the charge carriers to the surface as well as the recombination process involved by the electron-hole pairs in semiconductor particles. PL emission results from the radiative recombination of excited electrons and holes. In other words, it is a critical necessity of a good photocatalyst to have minimum electron-hole recombination. To study the recombination of charge carriers, PL studies of synthesized materials have been undertaken. PL emission intensity is directly related to recombination of excited electrons and holes. Fig. 23 shows the PL spectra of synthesized photocatalysts. It means TiO_2 and

Fig. 22. PL spectra of photocatalyst with TA (0.001 M) TiO_2, TiO_2/PPy, and $TiO_2/PPy/GO$.

Fig. 23. PL spectra of TiO_2, TiO_2/PPy, $TiO_2/PPy/GO$, PPy, and GO.

TiO_2/PPy with strong PL intensity have high recombination of charge carriers whereas $TiO_2/PPy/GO$ has weak intensity. The weak PL intensity of $TiO_2/PPy/GO$ may arise due to the coating of PPy on titania lattice, so that decrease in the band gap of $TiO_2/PPy/GO$ was found, which results in the decolourisation of photoexcited electrons. This delays the electrons-hole recombination process and hence is utilized in the redox reaction leading to improved photocatalytic activity [24].

3.12. Adsorption of dyes

The photodegradation of Victoria Blue and Rose Bengal dyes was done under visible-light irradiation in presence of TiO_2, TiO_2/PPy, and $TiO_2/PPy/GO$ nanocomposites. It is an example of heterogeneous catalysis. Rate laws in such reactions seldom follow proper law model and hence are inherently more difficult to formulate from the data. It has been widely accepted that heterogeneous catalytic reactions can be analyzed with the help of Langmuir Hinshelwood (LH) model [73,74], satisfying the following assumptions (i) there are limited number of adsorption sites on the catalyst and its surface is homogeneous, (ii) only one molecule can be adsorbed on one site and monolayer formation occurs, (iii) the absorption reaction is reversible in nature, and (iv) the adsorbed molecules do not react amongst themselves [75,76]. According to LH Model, following three steps take place in the kinetics mechanism [77,78]; these steps are of adsorption, surface reaction, and desorption of products from the surface.

Step 1: D (Dye) + C (catalyst) $\leftrightarrow$ D.C $\qquad$ (Adsorption)

Step 2: D.C $\leftrightarrow$ E.C + Other products $\qquad$ (Surface reaction)

Step 3: E.C $\leftrightarrow$ E + C $\qquad$ (Desorption)

The Freundlich isotherm [79] is employed, assuming a heterogeneous surface with a non-uniform distribution of heat of adsorption over the surface, and it may be written as:

$$q_e = K_F C_e^{\frac{1}{n}} \tag{7}$$

The above equation can be linearized as:

$$\ln q_e = \ln K_F + \frac{1}{n} \ln C_e \tag{8}$$

where q_e (mg/g) is the amount of solute adsorbed per unit weight of adsorbent; C_e (mg/L) is the equilibrium concentration of solute; K_F (mg/g) is the Freundlich constant (which indicate the relative adsorption capacity of the adsorbent); and $1/n$ is the constant indicate the intensity of adsorption. Since the photocatalyst is covered by both dye as well as water molecules (C_{water}) by hydrogen bonding, their competition for the active sites cannot be ignored.

Langmuir adsorption model [80] can be applied to the aqueous solutions of dyes with the help of the following expression:

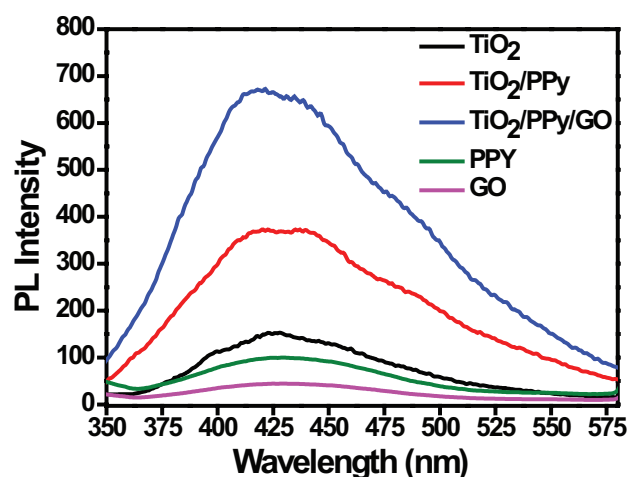$$q = \frac{q_t}{q_{max}} = \frac{K_L C}{1 + K_L C + K_{water} + C_{water}} \tag{9}$$
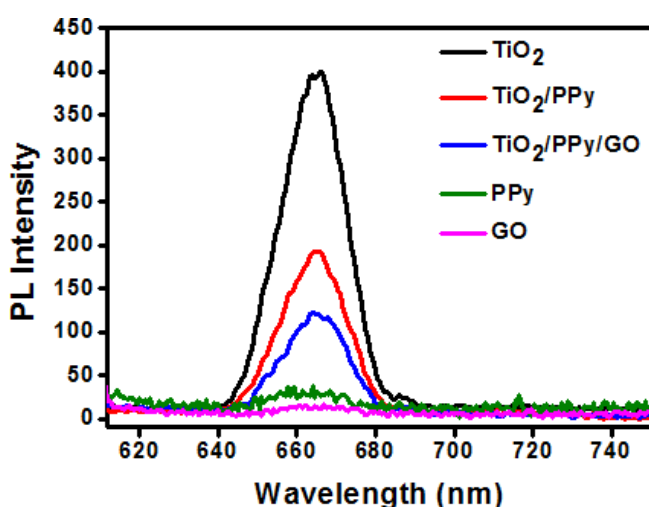
where q is the fractional sites covered by the dye; q_t is the absorbed quantity of dye at any time; q_{max} shows the maximum quantity of dye that can be adsorbed; K_L is the Langmuir adsorption constant for reactant; and K_{water} is the adsorption constant for water. The value of $C_{water} \gg C$; hence, C_{water} remains almost same throughout the reaction; and the catalyst coverage by water molecules remains almost constant. Thus, we can ignore the quantity K_{water} and C_{water}, and rewrite Eq. (9) as:

$$q = \frac{K_L C}{1 + K_L C} \tag{10}$$

The quantity adsorbed at a particular time can also be expressed as:

$$q_t = \frac{(\text{Reactor Volume}) \times (\text{Change in concentration})}{\text{Mass of catalyst}} \tag{11}$$

The equilibrium adsorption quantity q_{eq} can be written as:

$$q_e = q_{max} \left[\frac{K_L C_e}{1 + K_L C_e} \right] \tag{12}$$

where C_e is the equilibrium concentration of the dye. On transforming Eq. (12), a function can be derived as follows:

$$\frac{C_e}{q_e} = \frac{1}{K_L q_{max}} + \frac{C_e}{q_{max}} \tag{13}$$

The intercept on the vertical axis gives $1/K_L q_{max}$, and the reciprocal of slope gives q_{max}.

3.13. Kinetic study of photocatalytic degradation

For kinetic study of photocatalytic degradation, a control experiment was first carried out under two conditions, vis. (i) dye + visible light (no catalyst) and (ii) catalyst + dye in dark without any irradiation (Fig. 24). It can be seen that in under dark conditions, the amount of catalyst adsorbed becomes

constant after 20 min, where adsorption equilibrium is achieved. For the kinetic study of bleaching of Victoria Blue and Rose Bengal, the initial concentration of the dyes was varied, and the experiments were first conducted in dark for 20 min and then immediately followed by irradiation (Fig. 24). The amount of catalyst was kept constant (0.2 g) throughout the experiment.

Applying the LH model for determining the oxidation rate of the photocatalysis of dye:

$$\text{Rate}(r) = -\frac{dC}{dt} = k\theta = \theta = \frac{kK_A C}{1 + K_A C} \tag{14}$$

where k is the rate constant (mg/L min^{-1}); C is the concentration of dye; K_A is the adsorption constant of the dye (L/mg); and t is the illumination time (min).

During the course of the reaction, the initial pH, the amount of catalyst, and photo intensity were kept same. In addition to it, the formation of intermediates may interfere in the rate determination; hence, the calculation was done at the beginning of irradiation. The rate expression can be written as:

$$r_o = \frac{kK_A C_o}{1 + K_A C_o} \tag{15}$$

where r_0 is the initial rate of degradation of Victoria Blue and Rose Bengal, and C_0 is the initial concentration (almost equal to C_{eq}). When the initial concentration $C_{initial}$ is very small, C_0 will also be small, and Eq. (15) can be simplified as first-order equation [81,82]:

$$-\frac{dC}{dt} = kK_A C_o = \frac{\ln C_o}{C} = kK_A t \tag{16}$$

$$C = C_o e^{-k_f \text{photo} \, t} \tag{17}$$

where:

$$k_{f,\text{Photo}} = k \, k_A$$
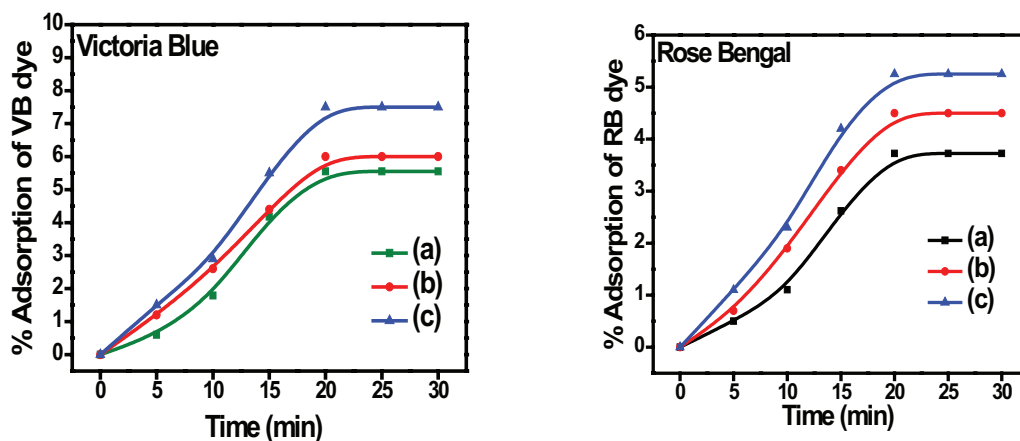

Fig. 24. Percentage of adsorption of Victoria Blue and Rose Bengal dye under dark condition in presence of: (a) TiO$_2$, (b) TiO$_2$/PPy, and (c) TiO$_2$/PPy/GO.

The value of $k_{f,photo}$ can be determined from the plot of ln C_t/C_0 vs. t (Fig. 25).

The slope of the straight line obtained will be the value of first-order rate constant [83]. The value of apparent rate constant was determined at definite concentrations of dye solution for photocatalysis reaction in presence of TiO_2, TiO_2/PPy, and TiO_2/PPy/GO shown in Fig. 25. The rate constant values for the photocatalytic degradation of Victoria Blue and Rose Bengal follow the first-order kinetic for both photocatalysts. This is confirmed that photocatalytic degradation of Victoria Blue and Rose Bengal follows first-order kinetic in presence of TiO_2, TiO_2/PPy, and TiO_2/PPy/GO.

3.14. Mechanism of photo-oxidation process

The acceleration of a chemical transformation by the presence of a catalyst with light is called photocatalysis. The catalyst may accelerate the photoreaction by interaction with the substrate in its ground or excited state and/or with a primary photoproduct, depending upon the mechanism of the photoreaction, itself remaining unaltered at the end of each catalytic cycle. Heterogeneous photocatalysis is a process in which two active phases, solid and liquid, are present. The solid phase is a catalyst, usually a semiconductor. The molecular orbital of semiconductors has a band structure. The bands of interest in photocatalysis are the populated valence band (Victoria Blue and Rose Bengal), and it is largely vacant CB, which is commonly characterized by the band gap energy (E_{bg}). The semiconductors may be photo-excited to form electron-donor sites (reducing sites) and electron acceptor sites (oxidizing sites), providing great scope for the redox reaction. When the semiconductor is illuminated with light (hn) of greater energy than that of the band gap, an electron is promoted from the Victoria Blue and Rose Bengal to the CB leaving a positive hole in the valence band and an electron in the CB as illustrated in Figs. 26 and 27.

If charge separation is maintained, the electron and hole may migrate to the catalyst surface where they participate in redox reactions with absorbed species. Specially, h^+ and
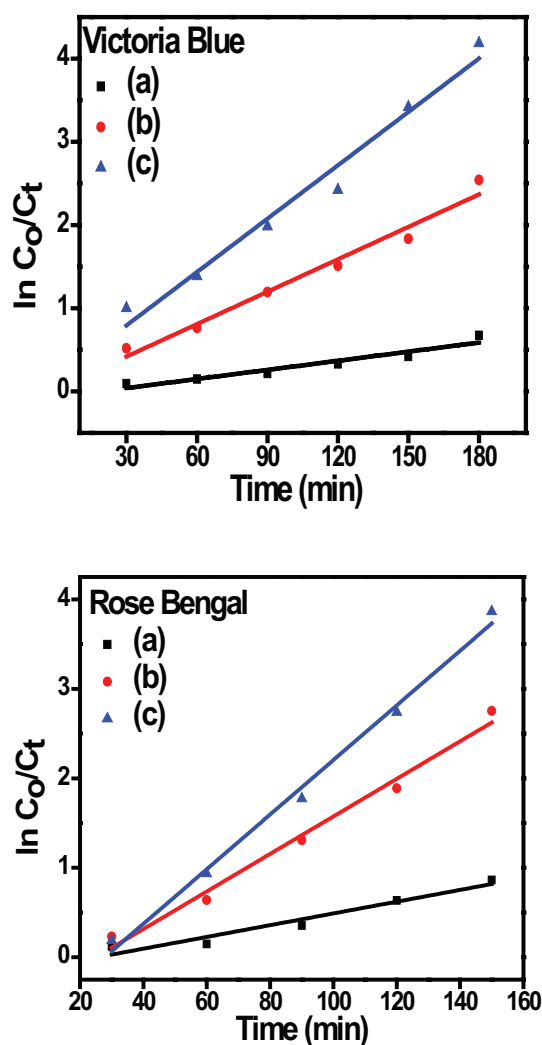

Fig. 25. Linear first-order reaction of LH kinetics of Victoria Blue and Rose Bengal dye vs. time: (a) TiO_2, (b) TiO_2/PPy, and (c) TiO_2/PPy/GO.
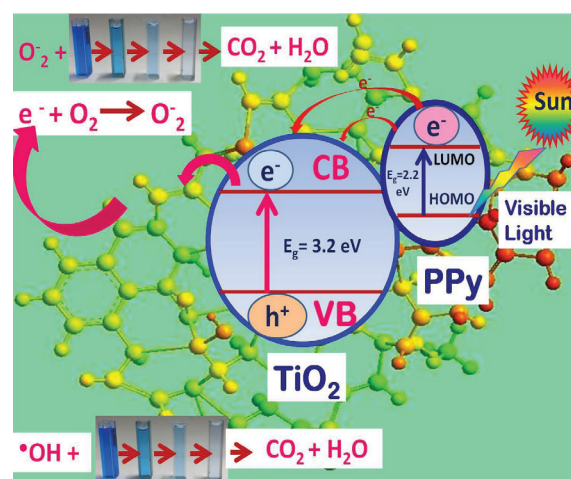

Fig. 26. Mechanism of photodegradation of Victoria Blue dye by TiO_2/PPy/GO nanocomposite.
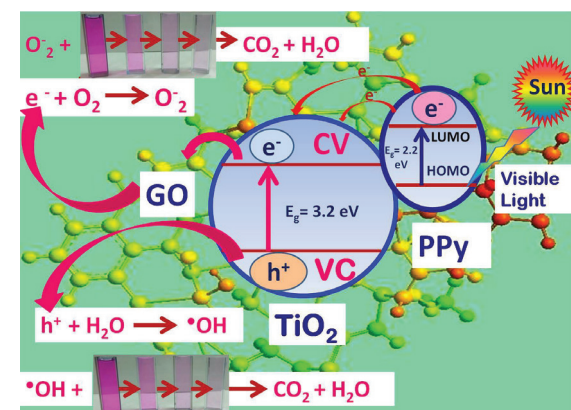

Fig. 27. Mechanism of photodegradation of Rose Bengal dye by TiO_2/PPy/GO nanocomposite.

dyes (Victoria Blue and Rose Bengal) may react with surface-bound H_2O or OH^- to produce the hydroxyl radical and e_{cb}^- is picked up by oxygen to generate superoxide radical anion (O_2^-), as indicated in the following Eqs. (18–20):
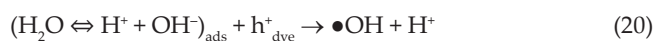
Absorption of efficient photons by titania:

$$(h\nu \geq E_{bg} = 3.2 \text{ eV})$$

$$TiO_2 + h\nu \rightarrow e_{cb} + h^+_{dye} \tag{18}$$

Formation of superoxide radical anion:

$$O_2 + e_{cb} \rightarrow O_2^- \tag{19}$$

Neutralization of OH^- group into OH by the hole:

$$(H_2O \Leftrightarrow H^+ + OH^-)_{ads} + h^+_{dye} \rightarrow \bullet OH + H^+ \tag{20}$$

It has been suggested that the hydroxyl radical ($\bullet$OH) and superoxide radical anions (O_2^-) are the primary oxidizing species in the photocatalytic oxidation processes [84,85]. These oxidative reactions would results in the degradation of the pollutants as shown in the following Eqs.(21 and 22):

Oxidation of the organic pollutants via successive attack by OH radicals:

$$R + \bullet OH \rightarrow R + H_2O \tag{21}$$

or by direct reaction with holes:

$$R + h^+ \rightarrow R^+ \rightarrow \text{degradation products} \tag{22}$$

4. Conclusions

The present research work describes a proficient method for synthesis of TiO_2/PPy and TiO_2/PPy/GO nanocomposites. These nanocomposites were prepared by one-step in-situ deposition oxidative polymerization of pyrrole hydrochloride using APS as an oxidant in the presence of ultra-fine grade powder of TiO_2 NPs cooled in an ice bath. The obtained nanocomposites were characterized by XRD, TEM, SEM, and UV-Vis for band gap determination. The obtained results showed that TiO_2 NPs have been encapsulated by PPy with a strong effect on the morphology of TiO_2/PPy and TiO_2/PPy/GO nanocomposites. The Photocatalytic degradation of Rose Bengal and Victoria Blue dye was done at different condition viz concentration of dye, time of illumination, pH, and dose of the photocatalyst. The maximum photodegradation was found at 7 pH; 20 ppm concentration of Victoria Blue and 25 ppm of Rose Bengal dye solution; 800 mg/L for VB and 1,600 mg/L for RB amount of photocatalyst; and 120 min irradiation of visible light. Kinetics of photodegradation was investigated for Victoria Blue and Rose Bengal dye and found first-order kinetics. The coating of PPy and GO has enhanced the photocatalytic activity of Titania. Hence, TiO_2/PPy and TiO_2/PPy/GO are the efficient photocatalyst for the degradation of Rose Bengal and Victoria Blue dye than pure TiO_2.

References

[1] J. Kaur, S. Singhal, Heterogeneous photocatalytic degradation of Rose Bengal: effect of operational parameters, Physica B, 450 (2014) 49–53.

[2] M.A. Fox, D.F. Duxbury, The photochemistry and photophysics of triphenylmethane dyes in solid and liquid media, Chem. Rev., 93 (1993) 381–433.

[3] S.K. Kansal, M. Singh, D. Sud, Studies on photodegradation of two commercial dyes in aqueous phase using different photocatalysts, J. Hazard. Mater., 141 (2007) 581–590.

[4] W. Azmi, R.K. Sani, U.C. Banerjee, Biodegradation of triphenylmethane dyes, Enzyme Microb. Technol., 22 (1998) 185–191.

[5] O.K. Dalrymple, D.H. Yeh, M.A. Trotz, Removing pharmaceuticals and endocrine-disrupting compounds from wastewater by photocatalysis, J. Chem. Technol. Biotechnol., 82 (2007) 121–134.

[6] F. Deng, L. Min, X. Luo, S. Wu, S. Luo, Visible-light photocatalytic degradation performances and thermal stability due to the synergetic effect of TiO_2 with conductive copolymers of polyaniline and polypyrrole, Nanoscale, 5 (2013) 8703–8710.

[7] S. Xu, Y. Zhu, L. Jiang, Y. Dan, Visible light induced photocatalytic degradation of methyl orange by polythiophene/TiO_2 composite particles, Water, Air, Soil Pollut., 213 (2010) 151–159.

[8] Y. Park, S. Lee, S.O. Kang, W. Choi, Organic dye-sensitized TiO_2 for the redox conversion of water pollutants under visible light, Chem. Commun., 46 (2010) 2477–2479.

[9] M. Saquib, M. Muneer, TiO_2-mediated photocatalytic degradation of a triphenylmethane dye (gentian violet), in aqueous suspensions, Dyes Pigm., 56 (2003) 37–49.

[10] X. Li, G. Liu, J. Zhao, Two competitive primary processes in the photodegradation of cationic triaryl methane dyes under visible irradiation in TiO_2 dispersions, New J. Chem., 23 (1999) 1193–1196.

[11] C.C. Chen, C.S. Lu, Photocatalytic degradation of Basic Violet 4: degradation efficiency, product distribution, and mechanisms, J. Phys. Chem. C, 111 (2007) 13922–13932.

[12] M. Okano, K. Itoh, A. Fujishima, K. Honda, Photoelectrochemical polymerization of pyrrole on TiO_2 and its application to conducting pattern generation, J. Electrochem. Soc., 134 (1987) 837–841.

[13] B. Wang, C. Li, J. Pang, X. Qing, J. Zhai, Q. Li, Novel polypyrrole-sensitized hollow TiO_2/fly ash cenospheres: synthesis, characterization, and photocatalytic ability under visible light, Appl. Surf. Sci., 258 (2012) 9989–9996.

[14] X. Chen, S.S. Mao, Titanium dioxide nanomaterials: synthesis, properties, modifications, and applications, Chem. Rev., 107 (2007) 2891–2959.

[15] A.L. Linsebigler, G. Lu, J.T. Yates, Photocatalysis on TiO_2 surfaces: principles, mechanisms, and selected results, Chem. Rev., 95 (1995) 735–758.

[16] R.J. Davis, J.L. Gainer, G.O. Neal, I.W. Wu, Photocatalytic decolorization of wastewater dyes, Water Environ. Res., 66 (1994) 50–53.

[17] S. Mozia, A.W. Morawski, M. Toyoda, M. Inagaki, Application of anatase-phase TiO_2 for decomposition of azo dye in a photocatalytic membrane reactor, Desalination, 241 (2009) 97–105.

[18] H. Tai, Y. Jiang, G. Xie, J. Yu, M. Zhao, Self-assembly of TiO_2/polypyrrole nanocomposite ultrathin films and application for an NH_3 gas sensor, Int. J. Environ. Anal. Chem., 87 (2007) 539–551.

[19] C.M. Ng, P.C. Chen, S. Manickam, Hydrothermal crystallization of titania on silver nucleation sites for the synthesis of visible light nano-photocatalysts—enhanced photoactivity using Rhodamine 6G, App. Catal., A, 433–434 (2012) 75–80.

[20] P.V. Kamat, K. Vinodgopal, D.E. Wynkoop, Environmental photochemistry on semiconductor surfaces: photosensitized degradation of a textile azo dye, acid orange 7, on TiO_2 particles using visible light, Environ. Sci. Technol., 30 (1996) 1660–1666.

[21] H. Huang, M. Gan, L. Ma, L. Yu, H. Hu, F. Yang, Y. Li, C. Ge, Fabrication of polyaniline/graphen/titania nanotube arrays nanocomposites and their application in supercapacitors, J. Alloys Compd., 630 (2015) 214–221.

[22] Y. Li, Y. Yu, L. Wu, J. Zhi, Processable polyaniline/titania nanocomposites with good photocatalytic and conductivity properties prepared via peroxo-titanium complex catalyzed emulsion polymerization approach, Appl. Surf. Sci., 273 (2013) 135–143.

[23] Y. Yang, J. Wen, J. Wei, R. Xiong, J. Shi, C. Pan, Polypyrrole-decorated Ag–TiO$_2$ nanofibers exhibiting enhanced photocatalytic activity under visible-light illumination, Appl. Mater. Interfaces, 5 (2013) 6201–6207.

[24] M. Vautier, C. Guillard, J.M. Herrmann, Photocatalytic degradation of dyes in water: case study of Indigo and of Indigo Carmine, J. Catal., 201 (2001) 46–59.

[25] G.K. Mor, K. Shankar, M. Paulose, O.K. Varghese, C.A. Grimes, Use of highly-ordered TiO$_2$ nanotube arrays in dye-sensitized solar cells, Nano Lett., 6 (2006) 215–218.

[26] T.L. Thompson, J.T. Yates, Surface science studies of the photoactivation of TiO$_2$ new photochemical processes, Chem. Rev., 106 (2006) 4428–4453.

[27] A. Kaur, Y.R. Smith, V.R. Subramanian, Improved photocatalytic degradation of textile dye using titanium dioxide nanotubes formed over titanium wires, Environ. Sci. Technol., 43 (2009) 3260–3265.

[28] W. Baran, A. Makowski, W. Wardas, The influence of FeCl$_3$ on the photocatalytic degradation of dissolved azo dyes in aqueous TiO$_2$ suspensions, Chemosphere, 53 (2003) 87–95.

[29] S. Wei, P. Mavinakuli, Q. Wang, D. Chen, R. Asapu, Y. Mao, N. Haldolaarachchige, D.P. Young, Z. Guo, Polypyrrole-titania nanocomposites derived from different oxidants, J. Electrochem. Soc., 158 (2011) K205–K212.

[30] J.S. Miller, Rose Bengal-sensitized photooxidation of 2-chlorophenol in water using solar simulated light, Water Res., 39 (2005) 412–422.

[31] B. Pare, P. Singh, S.B. Jonnalgadda, Degradation and mineralization of Victoria Blue B dye in a slurry photo reactor using advanced oxidation process, J. Sci. Ind. Res., 68 (2009) 724–729.

[32] J.L. Gole, J.D. Stout, C. Burda, Y. Lou, X. Chen, Highly efficient formation of visible light tunable TiO$_2$-XnX photocatalysts and their transformation at the nanoscale, J. Phys. Chem. B, 108 (2004) 1230–1240.

[33] J.D. Kwon, P.H. Kim, J.H. Keum, J.S. Kim, Polypyrrole/titania hybrids: synthetic variation and test for the photovoltaic materials, Sol. Energy Mater. Sol. Cells, 83 (2004) 311–321.

[34] D. Wang, Y. Wang, X. Li, Q. Luo, J. An, J. Yue, Sunlight photocatalytic activity of polypyrrole–TiO$_2$ nanocomposites prepared by 'in situ' method, Catal. Commun., 9 (2008) 1162–1166.

[35] H.C. Liang, X.Z. Li, Visible-induced photocatalytic reactivity of polymer–sensitized titania nanotube films, Appl. Catal., B, 86 (2009) 8–17.

[36] C. Ferreira, S. Domenech, P. Lacaze, Synthesis and characterization of poly-pyrrole/TiO$_2$ composites on mild steel, J. Appl. Electrochem., 31 (2001) 49–56.

[37] L. Sun, Y. Shi, B. Li, X. Li, Y. Wang, Preparation and characterization of polypyrrole/TiO$_2$ nanocomposites by reverse microemulsion polymerization and its photocatalytic activity for the degradation of methyl orange under natural light, Polym. Compos., 34 (2013) 1076–1080.

[38] Z. Guo, K. Shin, A.B. Karki, D.P. Young, R.B. Kaner, H.T. Hahn, Fabrication and characterization of iron oxide nanoparticles filled polypyrrole nanocomposites, J. Nanopart. Res., 11 (2009) 1441–1452.

[39] D.C. Marcano, D.V. Kosynkin, J.M. Berlin, A. Sinitskii, Z. Sun, A. Slesarev, L.B. Alemany, W. Lu, J.M. Tour, Improved synthesis of graphene oxide, ACS Nano, 4 (2010) 4806–4814.

[40] F. Denga, Y. Li, X. Luo, L. Yang, X. Tu, Preparation of conductive polypyrrole/TiO$_2$ nanocomposite via surface molecular imprinting technique and its photocatalytic activity under simulated solar light irradiation, Colloids Surf., A, 395 (2012) 183–189.

[41] M.C. Arenas, L.F. Nunez, D. Rangel, O.M. Alvarez, C.M. Alonso, V.M. Castano, Simple one-step ultrasonic synthesis of anatase titania/polypyrrole nanocomposites, Ultrason. Sonochem., 20 (2013) 777–784.

[42] M. Sedla, M. Mrlik, V. Pavlinek, P. Saha, O. Quadrat, Electrorheological properties of suspensions of hollow globular titanium oxide/polypyrrole particles, Colloid. Polym. Sci., 290 (2012) 41–48.

[43] K. Singh, R. Bharose, S.K. Verma, V.K. Singh, Potential of powdered activated mustard cake for decolorising raw sugar, J. Sci. Food Agric., 93 (2013) 157–165.

[44] H. Lachheb, E. Puzenat, A. Houas, M. Ksibi, E. Elaloui, C. Guillard, J.M. Herrmann, Photocatalytic degradation of various types of dyes (Alizarin S, Crocein Orange G, Methyl Red, Congo Red, Methylene Blue) in water by UV-irradiated titania, Appl. Catal., B, 39 (2002) 75–90.

[45] G.A. Epling, C. Lin, Photoassisted bleaching of dyes utilizing TiO$_2$ and visible light, Chemosphere, 46 (2002) 561–570.

[46] B.D. Cullity, S.R. Stock, Elements of X-Ray Diffraction, 3rd Ed., Prentice-Hall, Inc., New Jersey, 2001.

[47] M. Hema, A.Y. Arasi, P. Tamilselvi, R. Anbarasan, Titania nanoparticles synthesized by sol–gel technique, Chem. Sci. Trans., 2 (2013) 239–245.

[48] M.M. Ba-Abbad, A.A.H. Kadhum, A.B. Mohamad, M.S. Takriff, K. Sopian, Synthesis and catalytic activity of TiO$_2$ nanoparticles for photochemical oxidation of concentrated chlorophenols under direct solar radiation, Int. J. Electrochem. Sci., 7 (2012) 4871–4888.

[49] L. Cavigli, F. Bogani, A. Vinattieri, V. Faso, G. Baldi, Volume versus surface-mediated recombination in anatase TiO$_2$ nanoparticles, J. Appl. Phys., 106 (2009) 053516.

[50] S. Yang, X. Yang, X. Shao, R. Niu, L. Wang, Activated carbon catalyzed persulfate oxidation of Azo dye acid orange 7 at ambient temperature, J. Hazard. Mater., 186 (2011) 659–666.

[51] K.M. Reddy, S.V. Manorama, A.R. Reddy, Bandgap studies on anatase titanium dioxide nanoparticles, Mater. Chem. Phys., 78 (2002) 239–245.

[52] S. Bashir, J. Liu, H. Zhang, X. Sun, J. Guo, Band gap evaluations of metal-inserted titania nanomaterials, J. Nanopart. Res., 15 (2013) 1572.

[53] J. Guo, Interface science in nanoparticles: an electronic structure view of photon-in/photon-out soft-X-ray spectroscopy, Int. J. Quantum Chem., 109 (2009) 2714–2721.

[54] A. Achilleos, E. Hapeshi, N.P. Xekoukoulotakis, D. Mantzavinos, D.F. Kassinos, Factors affecting diclofenac decomposition in water by UV-A/TiO$_2$ photo-catalysis, Chem. Eng. J., 161 (2010) 53–59.

[55] K.M. Reza, A.S.W. Kurny, F. Gulshan, Parameters affecting the photocatalytic degradation of dyes using TiO$_2$: a review, Appl. Water Sci., 7 (2017) 1569–1578.

[56] E. Vulliet, J.M. Chovelon, C. Guillard, J.M. Herrmann, Factors influencing the photo-catalytic degradation of sulfonylurea herbicides by TiO$_2$ aqueous suspension, J. Photochem. Photobiol., A, 159 (2003) 71–79.

[57] K. Bubacz, J. Choina, D. Dolat, A.W. Morawski, Methylene blue and phenol photo-catalytic degradation on nanoparticles of anatase TiO$_2$, Pol. J. Environ. Stud., 19 (2010) 685–691.

[58] C.M. Ling, A.R. Mohamed, S. Bhatia, Performance of photocatalytic reactors using immobilized TiO$_2$ film for the degradation of phenol and methylene blue dye present in water stream, Chemosphere, 57 (2004) 547–554.

[59] C. Guillard, H. Lachheb, A. Houas, M. Ksibi, E. Elaloui, J.M. Herrmann, Influence of chemical structure of dyes, of pH and of inorganic salts on their photocatalytic degradation by TiO$_2$ comparison of the efficiency of powder and supported TiO$_2$, J. Photochem. Photobiol., A, 158 (2003) 27–36.

[60] B. Zielinska, J. Grzechulska, R.J. Kalenczuk, A.W. Morawski, The pH influence on photocatalytic decomposition of organic dyes over A11 and P25 titanium dioxide, Appl. Catal., B, 45 (2003) 293–300.

[61] S. Senthilkumaar, K. Porkodi, R. Gomathi, A.G. Maheswari, N. Manonmani, Sol–gel derived silver doped nanocrystalline titania catalysed photodegradation of methylene blue from aqueous solution, Dyes Pigm., 69 (2006) 22–30.

[62] S.K. Kansal, N. Kaur, S. Singh, Photocatalytic degradation of two commercial reactive dyes in aqueous phase using nanophotocatalysts, Nanoscale Res. Lett., 4 (2009) 709–716.

[63] K. Tanaka, K. Padermpole, T. Hisanaga, Photocatalytic degradation of commercial azo dyes, Water Res., 34 (2000) 327–333.

[64] J. Grzechulska, A.W. Morawski, Photocatalytic decomposition of azo-dye acid black 1 in water over modified titanium dioxide, Appl. Catal., B, 36 (2002) 45–51.

[65] E. Vulliet, J.M. Chovelon, C. Guillard, J.M. Herrmann, Factors influencing the photocatalytic degradation of sulfonylurea herbicides by TiO_2 aqueous suspension, J. Photochem. Photobiol., A, 159 (2003) 71–79.

[66] L. Zhang, W. Zhang, R. Li, H. Zhong, Y. Zhao, Y. Zhang, X. Wang, Photo degradation of methyl orange by attapulgite–SnO_2–TiO_2 nanocomposites, J. Hazard. Mater., 171 (2009) 294–300.

[67] D. Chen, A.K. Ray, Photocatalytic kinetics of phenol and its derivatives over UV irradiated TiO_2, Appl. Catal., B, 23 (1999) 143–157.

[68] S. Ameen, H.K. Seo, M.S. Akhtar, H.S. Shin, Novel graphene/polyaniline nano-composites and its photocatalytic activity toward the degradation of Rose Bengal dye, Chem. Eng. J., 210 (2012) 220–228.

[69] T. Sinha, M. Ahmaruzzaman, Photocatalytic decomposition behavior and reaction pathways of organic compounds using Cu nanoparticles synthesized via a green route, Photochem. Photobiol. Sci., 15 (2016) 1272–1281.

[70] L. Zang, C.Y. Liu, X.M. Ren, Photochemistry of semiconductor particles. Part 4. Effects of surface condition on the photodegradation of 2,4-dichlorophenol catalysed by TiO_2 suspensions, J. Chem. Soc., Faraday Trans., 91 (1995) 917–923.

[71] F.D. Mai, C.S. Lu, C.W. Wu, C.H. Huang, J.Y. Chen, C.C. Chen, Mechanisms of photocatalytic degradation of Victoria Blue R using nano-TiO_2, Sep. Purif. Technol., 62 (2008) 423–436.

[72] B.D. Credico, I.R. Bellobono, M. D'Arienzo, D. Fumagalli, M. Redaelli, R. Scotti, F. Morazzon, Efficacy of the reactive oxygen species generated by immobilized TiO_2 in the photocatalytic degradation of diclofenac, Int. J. Photoenergy, 2015 (2015) 1–13.

[73] J. Eriksson, J. Svanfelt, L. Kronberg, A photochemical study of diclofenac and its major transformation products, Photochem. Photobiol., 86 (2010) 528–532.

[74] J. Zhang, Y. Nosaka, Mechanism of the OH radical generation in photocatalysis with TiO_2 of different crystalline types, J. Phys. Chem. C, 118 (2014) 10824–10832.

[75] R.W. Matthews, Kinetics of photocatalytic oxidation of organic solutes over titanium dioxide, J. Catal., 111 (1988) 264–272.

[76] R. Zepp, D. Crosby, A, Lewis Publs., CRC Press, Boca Raton, Florida, Chapter 22 (1994) 317–348.

[77] S. Yang, X. Yang, X. Shao, R. Niu, L. Wang, Activated carbon catalyzed persulfate oxidation of azo dye acid orange 7 at ambient temperature, J. Hazard. Mater., 186 (2011) 659–666.

[78] N. Guettaı, H.A. Amar, Photocatalytic oxidation of methyl orange in presence of titanium dioxide in aqueous suspension. Part II: Kinetics study, Desalination, 185 (2005) 439–448.

[79] E. Kordouli, K. Bourikas, A. Lycourghiotis, C. Kordulis, The mechanism of azo-dyes adsorption on the titanium dioxide surface and their photocatalytic degradation over samples with various anatase/rutile ratios, Catal. Today, 252 (2015) 128–135.

[80] I.K. Konstantinou, T.A. Albanis TiO_2-assisted photocatalytic degradation of azo dyes in aqueous solution: kinetics and mechanistic investigations. A review, Appl. Catal., B, 49 (2004) 1–14.

[81] A.F. Júnior, E.C. de Oliveira Lima, A.N. Miguel, P.R. Wells, Synthesis of nanoparticles of $Co_xFe_{(3-x)}O_4$ by combustion reaction method, J. Magn. Magn. Mater., 308 (2007) 198–202.

[82] M.A. Abu-Hassan, J.K. Kim, I.S. Metcalfe, D. Mantzavinos, Kinetics of low frequency sonodegradation of linear alkylbenzene sulfonate solutions, Chemosphere, 62 (2006) 749–755.

[83] N.M. Mahmoodi, M. Arami, N.Y. Limaee, N.S. Tabrizi, Kinetics of heterogeneous photocatalytic degradation of reactive dyes in an immobilized TiO_2 photocatalytic reactor, J. Colloid Interface Sci., 295 (2006) 159–164.

[84] G.M. Liu, X.Z. Li, J.C. Zhao, S. Horikoshi, H. Hidaka, Photooxidation mechanism of dye alizarin red in TiO_2 dispersions under visible illumination: an experimental and theoretical examination, J. Mol. Catal. A: Chem., 153 (2000) 221–229.

[85] C. Galindo, P. Jacques, A. Kalt, Photodegradation of the aminoazobenzene acid orange 52 by three advanced oxidation processes: UV/H_2O_2, UV/TiO_2 and VIS/TiO_2: comparative mechanistic and kinetic investigations, J. Photochem. Photobiol. A, 130 (2000) 35–47.